






Review

Macromolecular Design for Oxygen/Nitrogen Permselective Membranes—Top-Performing Polymers in 2020—

Jianjun Wang ¹, Zhichun Shi ², Yu Zang ¹, Hongge Jia ¹, Masahiro Teraguchi ³, Takashi Kaneko ³
and Toshiki Aoki ^{3,*}

¹ Key Laboratory of Polymeric Composition Material of Heilongjiang Province, College of Materials Science and Engineering, Qiqihar University, Wenhua Street 42, Qiqihar 161006, China; 02900@qqhru.edu.cn (J.W.); zangyu@qqhru.edu.cn (Y.Z.); 01723@qqhru.edu.cn (H.J.)

² Technology Innovation Center of Industrial Cannabis Processing of Heilongjiang Province, College of Chemistry and Chemical Engineering, Qiqihar University, Wenhua Street 42, Qiqihar 161006, China; 02897@qqhru.edu.cn

³ Department of Chemistry and Chemical Engineering, Graduate School of Science and Technology, Niigata University, Ikarashi 2-8050, Nishi-Ku, Niigata 950-2181, Japan; teraguti@eng.niigata-u.ac.jp (M.T.); kanetaka@gs.niigata-u.ac.jp (T.K.)

* Correspondence: toshaoki@eng.niigata-u.ac.jp

Abstract: Oxygen/nitrogen permselective membranes play particularly important roles in fundamental scientific studies and in a number of applications in industrial chemistry, but have not yet fulfilled their full potential. Organic polymers are the main materials used for such membranes because of the possibility of using sophisticated techniques of precise molecular design and their ready processability for making thin and large self-supporting membranes. However, since the difference in the properties of oxygen and nitrogen gas molecules is quite small, for example, their kinetic diameters are 3.46 Å and 3.64 Å, respectively, the architectures of the membrane macromolecules should be designed precisely. It has been reported often that oxygen permeability (P_{O_2}) and oxygen permselectivity ($\alpha = P_{O_2}/P_{N_2}$) have trade-off relationships for symmetric membranes made from pure polymers. Some empirical upper bound lines have been reported in $(\ln \alpha - \ln P_{O_2})$ plots since Robeson reported an upper bound line in 1991 for the first time. The main purpose of this review is to discuss suitable macromolecular structures that produce excellent oxygen/nitrogen permselective membranes. For this purpose, we first searched extensively and intensively for papers which had reported α and P_{O_2} values through symmetric dense membranes from pure polymers. Then, we examined the chemical structures of the polymers showing the top performances in $(\ln \alpha - \ln P_{O_2})$ plots, using their aged performances. Furthermore, we also explored progress in the molecular design in this field by comparing the best polymers reported by 2013 and those subsequently found up to now (2020) because of the rapid outstanding growth in this period. Finally, we discussed how to improve α and P_{O_2} simultaneously on the basis of reported results using not only symmetric membranes of pure organic polymers but also composite asymmetric membranes containing various additives.

Keywords: macromolecular design; oxygen/nitrogen separation; polymer membranes; top-performing polymers; upper bounds; oxygen permeability; oxygen permselectivity



Citation: Wang, J.; Shi, Z.; Zang, Y.; Jia, H.; Teraguchi, M.; Kaneko, T.; Aoki, T. Macromolecular Design for Oxygen/Nitrogen Permselective Membranes—Top-Performing Polymers in 2020—. *Polymers* **2021**, *13*, 3012. <https://doi.org/10.3390/polym13173012>

Academic Editor: Alessio Fuoco

Received: 21 June 2021

Accepted: 23 August 2021

Published: 6 September 2021

Publisher's Note: MDPI stays neutral with regard to jurisdictional claims in published maps and institutional affiliations.



Copyright: © 2021 by the authors. Licensee MDPI, Basel, Switzerland. This article is an open access article distributed under the terms and conditions of the Creative Commons Attribution (CC BY) license (<https://creativecommons.org/licenses/by/4.0/>).

1. Introduction

1.1. Significance of Oxygen/Nitrogen Permselective Membranes

Gas separation membranes are very important and have a promising future not only because of their scientific interest to chemists and scientists but also for their practical applications such as removal of contaminants and purification of resources important to chemical and materials engineers [1–8]. Therefore, intensive and continuous studies on gas separation membranes have been carried out for many years that have resulted

in some practical uses. In particular, oxygen/nitrogen permselective membranes are very important in both the industrial and medical fields. For example, they can be used to treat seriously ill patients with a pulmonary disease like COVID-19. However, the performances of gas separation membranes, especially for separating oxygen and nitrogen, are not as good as desired because their sizes and properties are very similar. For example, the kinetic diameters of an oxygen molecule and a nitrogen molecule are 3.46 Å and 3.64 Å, respectively, and this size difference is extremely small (0.18 Å). As materials for such membranes, soluble organic polymers are popular and useful because they can be fabricated very easily and economically as dense thin membranes without any void defects through which gas molecules can pass freely without any selectivity.

1.2. Requirements for Polymers as Oxygen/Nitrogen Permselective Membranes

There are mainly two requirements for polymers as permselective membranes for a gas mixture of oxygen/nitrogen as follows [1].

- (1) high processability, mechanical strength, and stability
- (2) high oxygen permselectivity, that is, a high oxygen permeability coefficient (P_{O_2} (barrer)) and high oxygen separation factor ($\alpha = P_{O_2}/P_{N_2}$)

The oxygen permeability coefficient (P_{O_2} (barrer)) is the quantity (volume: cc(STP)) of oxygen gas molecules permeated through a polymer membrane normalized by the membrane area (cm²), membrane thickness (cm), permeation time (s), and pressure difference applied (driving force) (cmHg). The unit, barrer, is defined by 1 barrer = 1×10^{-10} cc (STP) cm cm⁻² s⁻¹ cmHg⁻¹, where STP means a standard temperature (25 °C) and pressure (1 atm). Since this is a characteristic value for each polymer architecture, this value basically depends on the macromolecular structure. However, different P_{O_2} values for polymers with the same first-order structures (chemical structures) were often reported because they could have different high-ordered structures (solid-state structures or membranes structures) even if the polymers had the same macromolecular structures.

There are two main trade-off problems concerning the requirements for good oxygen separation membrane materials as follows.

- (1) Polymers with higher regular structures which are needed for higher α values have lower processability because they are insoluble and vice versa.
- (2) Polymers with higher α values have lower P_{O_2} values and vice versa. (For the detail, see Section 1.4).

1.3. Mechanisms of Gas Permselective Membranes (Figure 1)

Because gas molecules are very small particles around 2.6–5.5 Å in kinetic diameter, membranes for gas separation should be dense (non-porous) or microporous and not have any defects whose sizes are more than several Å. Figure 1 summarizes three well-known permselective mechanisms useful for oxygen and nitrogen separation [1–8]. The details of the three are described below.

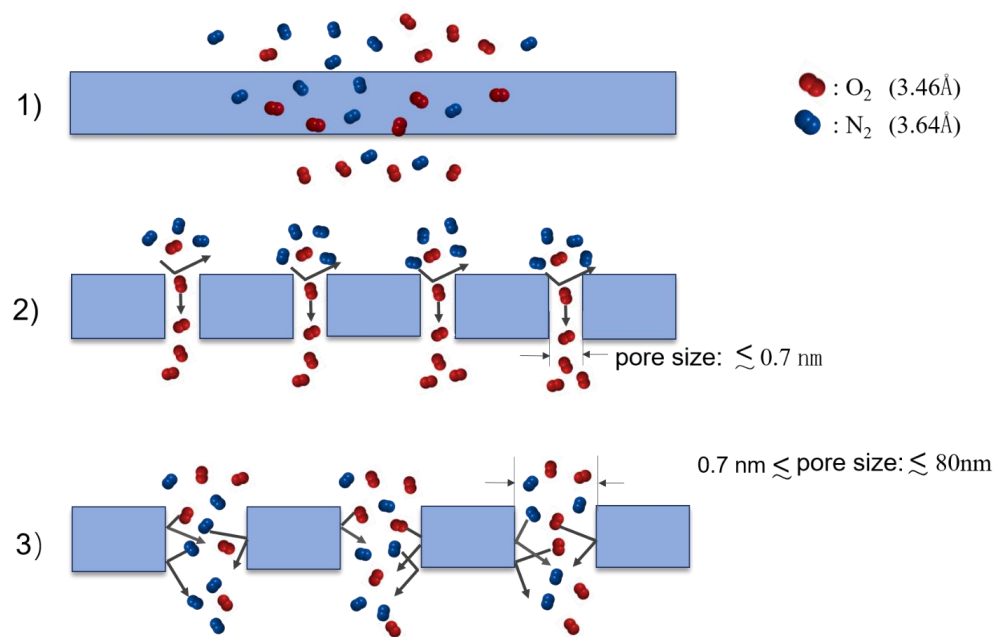


Figure 1. Mechanisms of oxygen selective permeation through membranes. (1) Solution-diffusion (SD) mechanism for dense (non-porous) membranes, (2) molecular-sieving (MS) mechanism for ultramicroporous membranes, (3) Knudsen (Kd) mechanism for microporous and mesoporous membranes.

1.3.1. Solution-Diffusion (SD) Mechanism for Dense (Non-Porous) Membranes

Dense (non-porous) membranes have no pores but gas molecules can permeate them. A popular and the simplest mechanism for gas permeation through dense membranes known as the solution-diffusion (SD) mechanism involves the following two-step process: (i) dissolution (or sorption) of permeating gas molecules on a membrane surface and then (ii) diffusion of the gas molecules across the membrane. In this simple model, the oxygen permeability coefficient (P_{O_2} : cc (STP) cm cm⁻² s⁻¹ cmHg⁻¹) is the product of the oxygen solubility coefficient (S_{O_2} : cc(STP) cm⁻³ cmHg⁻¹) and the oxygen diffusion coefficient (D_{O_2} : cm² s⁻¹).

$$P_{\text{O}_2} = S_{\text{O}_2} \times D_{\text{O}_2} \quad (1)$$

The oxygen permselectivity, α ($P_{\text{O}_2}/P_{\text{N}_2}$) is the product of the oxygen solubility selectivity (α_S ($=S_{\text{O}_2}/S_{\text{N}_2}$)) and the oxygen diffusion selectivity (α_D ($=D_{\text{O}_2}/D_{\text{N}_2}$)).

$$\alpha = \alpha_S \times \alpha_D \quad (2)$$

Therefore, oxygen separation of membranes based on the SD mechanism depends on the two factors, that is, dissolution (or sorption) selectivity α_S ($=S_{\text{O}_2}/S_{\text{N}_2}$) and diffusion selectivity α_D ($=D_{\text{O}_2}/D_{\text{N}_2}$). Although, in many of gas pairs, if $\alpha_S > 1$, $\alpha_D < 1$ and vice versa. However, in the case of oxygen/nitrogen, $\alpha_S > 1$ and $\alpha_D > 1$ generally.

1.3.2. Molecular-Sieving (MS) Mechanism for Ultramicroporous and Microporous Membranes

When one of the authors (T.A.) published a review article on macromolecular design for permselective membranes in 1999 [1], the molecular-sieving (MS) mechanism was not popular and most oxygen permselective membranes were discussed on the basis of the SD mechanism described above. Recently, it has been thought that this MS mechanism is important for realizing high performance for oxygen separation membranes. Because the sizes of an oxygen and a nitrogen molecule are 3.46 Å and 3.64 Å, respectively, it is ideally desired that static micropores whose sizes are smaller than around 5 Å are created in polymer membranes. However, for common polymers, since 5 Å is within the range of the thermal motion of their polymer backbones and polymer molecules can flex over this

range, it is not easy to create static pores whose sizes are less than 5 Å suitable for oxygen separation based on the MS mechanism.

The MS separation mechanism for an oxygen/nitrogen mixture may be applied to permeations through membranes containing micropores whose sizes are less than around 5–10 Å (0.5–1 nm) because the pore sizes should be less than 2–3 times of the size of the permeating gas molecule (0.346 nm). The IUPAC defined the terms “ultra-micropores” and “micropores” as small pores with sizes of less than 0.7 nm and 2 nm, respectively. Therefore, for highly oxygen permselective membranes based on the MS mechanism, ultra-micropores are appropriate and micropores are too large.

1.3.3. Knudsen (Kd) Mechanism for Microporous and Mesoporous Membranes

When pore sizes in a membrane are smaller than the mean free path (λ) of a permeant gas, the diffusion of the gas follows the Knudsen (Kd) mechanism, where the permeability coefficient is inversely proportional to the square root of the molecular weight of the gas. In the case of oxygen, its λ value is about 60–100 nm. Therefore, when separating oxygen using the membranes with pores whose sizes are from 5–10 Å (0.5–1 nm) to 60–100 nm follows the Knudsen (Kd) mechanism. Its permeation (diffusion) selectivity is expressed by the following equation.

$$\alpha (P_{O_2}/P_{N_2}) = \alpha_S (S_{O_2}/S_{N_2}) \times \alpha_D (D_{O_2}/D_{N_2}) \quad (3)$$

Because $\alpha_S (S_{O_2}/S_{N_2}) = 1$, in this case,

$$\alpha (P_{O_2}/P_{N_2}) = \alpha_D (D_{O_2}/D_{N_2}) = (M_{N_2})^{1/2}/(M_{O_2})^{1/2} = 0.93$$

Therefore, in the case of oxygen/nitrogen mixtures, nitrogen permeates predominantly through Knudsen (Kd) membranes. In addition, because α_S makes no contribution for this kind of membrane, separation by selective dissolution is not useful for the case of oxygen/nitrogen separation.

In conclusion, for oxygen permselective membranes, nonporous or ultramicroporous polymer membranes are suitable, that is, membranes with micropores whose sizes are from 5–10 Å (0.5–1 nm).

1.3.4. Transition Range between the Solution-Diffusion (SD) Mechanism for Dense (Non-Porous) Membranes, the Molecular-Sieving (MS) Mechanism for Ultra-Microporous Membranes, and the Knudsen (Kd) Mechanism for Microporous and Mesoporous Membranes

As described above, in the case of oxygen, permeation through membranes with pores whose sizes are less than 60–100 nm follows the Knudsen (Kd) mechanism, and separation based on the molecular-sieving (MS) mechanism for oxygen/nitrogen mixture requires micropores with sizes less than about 5–10 Å (0.5–1 nm). Baker also reported that the transition between the MS mechanism and the solution-diffusion (SD) mechanism is in the range of 0.5–1 nm [9]. In conclusion, the minimum and maximum sizes of actual pores in polymer membranes which can separate oxygen/nitrogen mixtures by the MS mechanism are around 5 Å and 10 Å, respectively.

1.4. Robeson's and Pinnau's Upper Bound Lines

1.4.1. Existence of Upper Bound Lines in Selectivity-Permeability Plots

In order to compare oxygen permselectivity, that is, P_{O_2} and $\alpha (=P_{O_2}/P_{N_2})$ for various membranes, many researchers used a plot of $\ln \alpha$ versus $\ln P_{O_2}$. In general, trade-off relationships between P_{O_2} and α are well-known. Prof. Robeson plotted many experimental values obtained from the literature and drew an upper bound line in 1991 as shown in Figure 2 [10]. This is the original upper bound line. In the 1991 figure, substituted acetylene polymers (PAs) including poly(1-trimethylsilylpropyne) (PTMSP, see Figure 2) and polyimides (PIs) were plotted as very high P_{O_2} polymers, and as high α polymers, respectively. The figure also showed that in general, glassy polymers showed better performances than rubbery polymers. The details are described in Section 2.1.

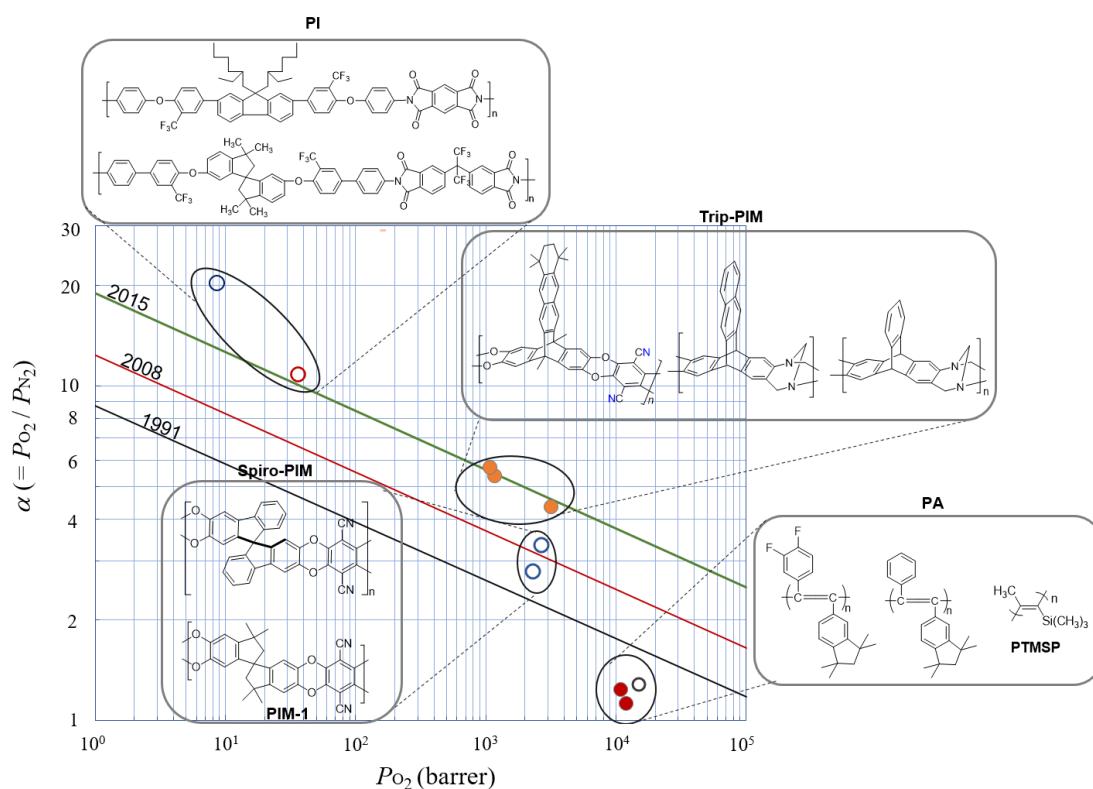


Figure 2. Robeson's 1991, 2008, and Pinnau's 2015 upper bound lines for oxygen/nitrogen permeation through polymer membranes with plots for milestone polymers (●: after aging, ○: before aging).

1.4.2. Meaning of the Upper Bound Lines—The Slope and Intercept

Although Robeson's 1991 upper bound line was drawn from empirical results, Prof. Freeman explained the theoretical meaning of the line in 1999 [11]. He constructed the following equation for the line:

$$\ln \alpha = -\mathbf{A} \ln P_{O_2} + \mathbf{B} \quad (4)$$

where **A** and **B** indicate the slope of the line and the intercept at $\ln P_{O_2} = 0$, respectively. He discussed the meaning of **A** and **B** in the following way.

$$\mathbf{A} = (d_{N_2}/d_{O_2})^2 - 1 = (3.64/3.46)^2 - 1 = 0.105 \quad (5)$$

where d_{O_2} and d_{N_2} are kinetic diameters for oxygen and nitrogen, respectively. Since the **A** value is determined by gas pairs as permeants, it has no relationship to the structures of the membrane polymers. Therefore, it cannot be improved by well-organized molecular design based on researchers' efforts. On the other hand, he proposed that the **B** value is affected by solubility selectivity and the structures of membrane polymers. Therefore, researchers can design new polymers showing good performances by controlling the **B** value. Furthermore, since the solubility selectivity is low in the case of oxygen/nitrogen, precise design of polymers to enhance α_D is more important. In order to obtain good performance of polymer membranes, that is, to realize a simultaneous increase in selectivity and permeability, it is effective to increase chain stiffness (main chain rigidity) and interchain spacing (fractional free volume (FFV)).

1.4.3. History of the Upper Bound Lines—From 1991 via 2008 to 2015

When one of the authors (T.A.) published a review article on macromolecular design for permselective membranes in 1999 [1], only Robeson's 1991 upper bound line was known. Since 1991, the upper line has been moving in the upper-right direction. For

example, Robeson's 2008 upper bound line [12] and Pinnau's 2015 upper bound line [13] were reported as shown in Figure 2. As Prof. Freeman predicted in 1999 [11], their slopes are the same as shown in Figure 2.

The advent of Robeson's 2008 upper bound line was caused by the emergence of a new type of polymer called PIM (polymers of intrinsic microporosity) such as PIM-1 as shown in Figure 2. This polymer backbone includes a rigid ladder structure consisting of alternating fused aromatic and aliphatic cycles with spiro-type carbons as kink points. In this review, we call this type of PIMs as Spiro-PIM. The details are described in Section 2.1.4.

Recently, Pinnau's 2015 upper bound line appeared. The new line was caused by the advent of another type of PIMs. Similar to a Spiro-PIM, these advanced new PIMs contain a rigid ladder structure consisting of alternating fused aromatic and aliphatic cycles. But instead of spiro-type carbons in Spiro-PIMs, they include triptycene groups as kink points (see Figure 2). In this review, we call this type of PIM the Trip-PIM. The details are described in Section 2.2.2.

1.4.4. Aging Problems for Ultrahigh Permeable Polymers

As described above, the ultramicropores which are needed for high performance of oxygen permselective membranes based on the molecular-sieving (MS) mechanism have a similar size to that of the thermal motion of the polymer backbone. In addition, because these pores are mainly present between macromolecules, they are usually unstable, particularly in the case of ultrahigh permeability polymers ($P_{O_2} > 10^3$) such as PTMSP (the details are described in Section 2.1.2). Therefore, they often showed an aging effect, whereby with increasing time their permeability significantly decreased. *Because we think that the stable values after aging are the real and intrinsic values of polymers, we plotted separately the aged values by solid symbols and transient non-aged values by open symbols in all the figures in this review whenever aged values were reported.*

1.4.5. Advantages and Disadvantages of Polymers as Materials for Oxygen/Nitrogen Permselective Membranes

As described in Section 1.1, soluble polymers are suitable for oxygen/nitrogen permselective membranes because they can be fabricated easily as dense thin membranes. This is the fundamental advantage of polymers. In addition, their chemical structures can be controlled with an accuracy of subnanometer order by organic and polymer synthesis. Therefore, it is possible to control precisely the size of the permeation path of oxygen and nitrogen. However, in the case of linear soluble polymers because permeation paths are mainly present between macromolecules, they are usually unstable (see Section 1.4.4) and it is difficult to control the size.

1.5. Purposes of This Review

The main aim of this review is to discuss how to design and obtain new good polymers with both high oxygen permeability (P_{O_2}) and oxygen permselectivity ($\alpha (P_{O_2}/P_{N_2})$). For this purpose, we first extensively searched for papers reporting values of α and P_{O_2} for polymers with well-defined chemical structures. Then, we selected polymers showing the highest α at each P_{O_2} among them. Finally, we plotted them on a $(\ln \alpha (P_{O_2}/P_{N_2}) - \ln P_{O_2})$ graph (see Section 2). As described above, if papers reported more than two values before and after aging for the same polymer, we plotted both values as open and solid symbols, respectively. In addition, in order to see the history of recent progress of the research for oxygen permeation polymers, results until 2013 and up to now (until 2020) are discussed separately in Sections 2.1 and 2.2, respectively. Furthermore, in Section 3, in order to discuss strategies for enhancing P_{O_2} and $\alpha (P_{O_2}/P_{N_2})$ simultaneously, we selected such examples from the literature although we found they were quite few. *While we described the performance of only pure polymers in Section 2, we included modified polymers such as composite polymers in Section 3 because of the very rare examples for pure polymers* (For the contents of this review, see Supplementary Materials S1).

Finally, by using these collected data of pure membranes from these top-performing linear soluble polymers and composite membranes including insoluble polymers whose P_{O_2} and $\alpha (P_{O_2}/P_{N_2})$ were simultaneously enhanced, we will summarize the relationships between the chemical structures and performances and discuss how to obtain new good polymers with high values for both P_{O_2} and α .

2. Macromolecular Design for Oxygen/Nitrogen Permselective Membranes—Top-Performing Polymers

2.1. Top-Performing Polymers until 2013 as Oxygen/Nitrogen Permselective Membranes

Figure 3 shows plots of top-performing polymers showing the highest α at each P_{O_2} reported in the literature until 2013. The values and categorization are listed in Table 1 [14–35]. The chemical structures of the polymers showing the best performances are shown in Chart 1. These polymers can be categorized into the following three groups. Group I: polymers 1–9 with the highest P_{O_2} and the lowest α below the 1991 upper line, Group II: polymers 10–16 with relatively high α and intermediate P_{O_2} beyond the 1991 upper line and close to, or on, the 2008 upper line, and Group III: polymers 17–23 with the highest α and the lowest P_{O_2} close to the 1991 upper line. Typical polymers categorized into Groups I, II, and III are poly (substituted acetylenes) (PAs) such as PTMSP, Spiro-PIMs (polymer of intrinsic microporosity with spiro-carbons), and polyimides (PIs), respectively. The details are described below.

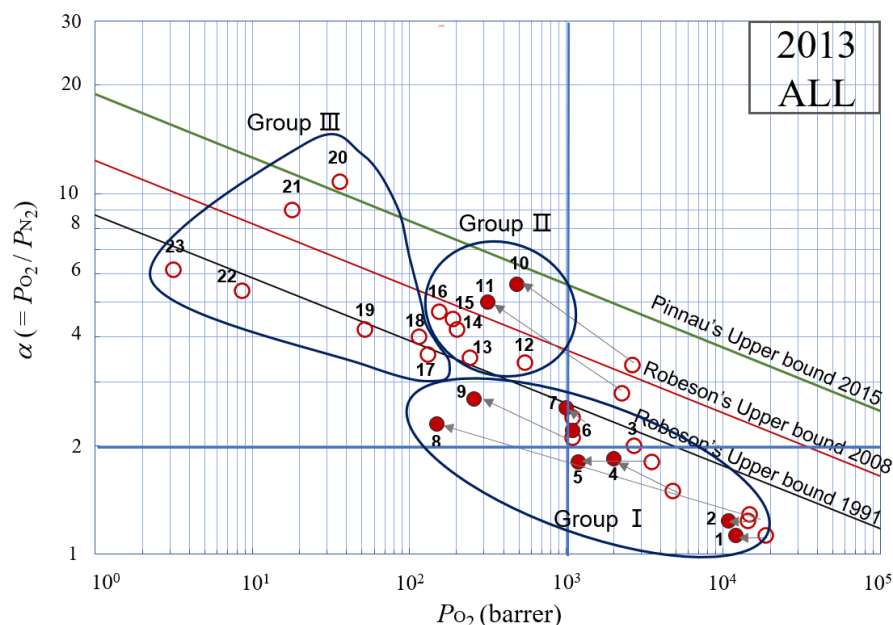


Figure 3. Plots of oxygen permselectivity through polymers, showing the highest α at each P_{O_2} reported in the literature until 2013 (●: after aging, ○: before aging). For the data and categorization of the plots, see Table 1, and for the chemical structures of the polymers in the plots, see Chart 1.

Table 1. Categorization and detailed data for membrane polymers in Figure 3 (All polymers until 2013).

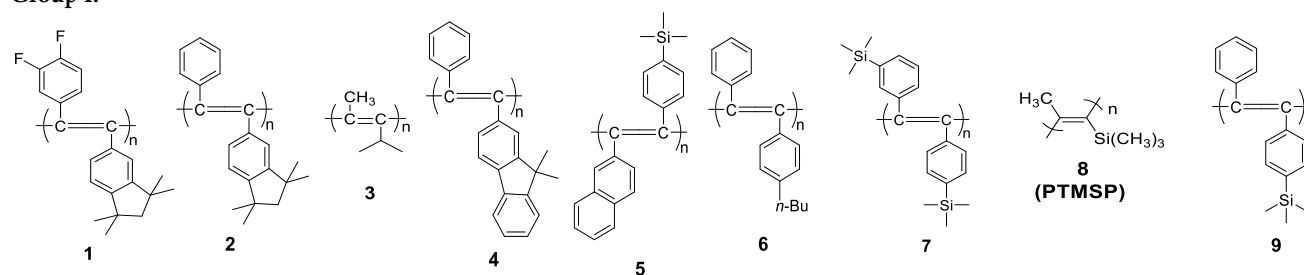
Code	Polymer Type	P_{O_2} (barrer)	$\alpha (=P_{O_2}/P_{N_2})$	Aging Time (days)	Thickness (μm)	Feed Gas	Ref. (year)
Group I							
1	PA	12,000 (18,700)	1.13 (1.13)	90	80–120	pure	[14] (2008)
2	PA	10,800 (14,400)	1.24 (1.24)	60	-	pure	[15] (2007)
3	PA	(2700)	(2.00)	-	20–40	pure	[16] (1996)

Table 1. Cont.

Code	Polymer Type	P_{O_2} (barrer)	$\alpha (=P_{O_2}/P_{N_2})$	Aging Time (days)	Thickness (μm)	Feed Gas	Ref. (year)
4	PA	2000 (4800)	1.84 (1.50)	90	80	pure	[17] (2009)
5	PA	1200 (3500)	1.80 (1.80)	90	-	pure	[18] (2006)
6	PA	1100	2.20	-	-	pure	[19] (1994)
7	PA	1000 (1100)	2.55 (2.40)	90	30–120	mixed	[20] (2002)
8	PA (PTMSP)	150 (14,800)	2.30 (1.29)	1460	-	pure	[21] (1993) [14] (2008)
9	PA	260 (1100)	2.70 (2.10)	26 h	-	-	[22] (1992)
Group II							
10	Spiro-PIM	486 (2640)	5.60 (3.35)	2088	100 180	pure pure	[23] (2018) [24] (2012)
11	Spiro-PIM (PIM-1)	317 (2270)	5.00 (2.80)	1380	128 -	pure pure	[25] (2015) [24] (2012)
12	Spiro-PIM-PI	(545)	(3.40)		96	pure	[26] (2008)
13	Spiro-PIM-PI	(243)	(3.50)		80–100	pure	[27] (2013)
14	Modified Spiro-PIM	(201)	(4.20)		70–90	pure	[28] (2009)
15	Spiro-PIM	(190)	(4.50)		28	pure	[29] (2005)
16	Modified Spiro-PIM	(156)	(4.70)		50–70	pure	[30] (2008)
Group III							
17	PI	(132)	(3.57)		50	pure	[31] (2001)
18	Spiro-PIM-PI	(116)	(4.00)		80–100	pure	[27] (2013)
19	PI	(52.0)	(4.20)		60	pure	[32] (2013)
20	Spiro-PIM-PI	(36.1)	(10.8)		85	pure	[33] (2010)
21	Spiro-PI	(18.0)	(9.00)		30–60	pure	[34] (2005)
22	PI	(8.60)	(5.38)		30–90	pure	[35] (1999)
23	Modified PI	(3.14)	(6.16)		60	mixed	[32] (2013)

[Note] Data in parentheses are those before aging. For the codes for polymers, see, Chart 1. For the codes for polymer types, see the text.

Group I:



Group II:

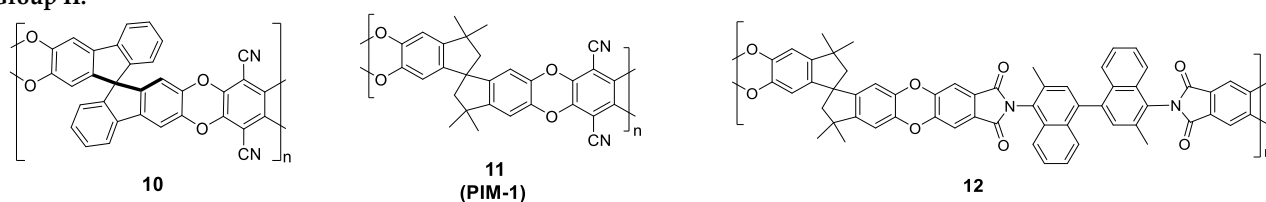


Chart 1. Cont.

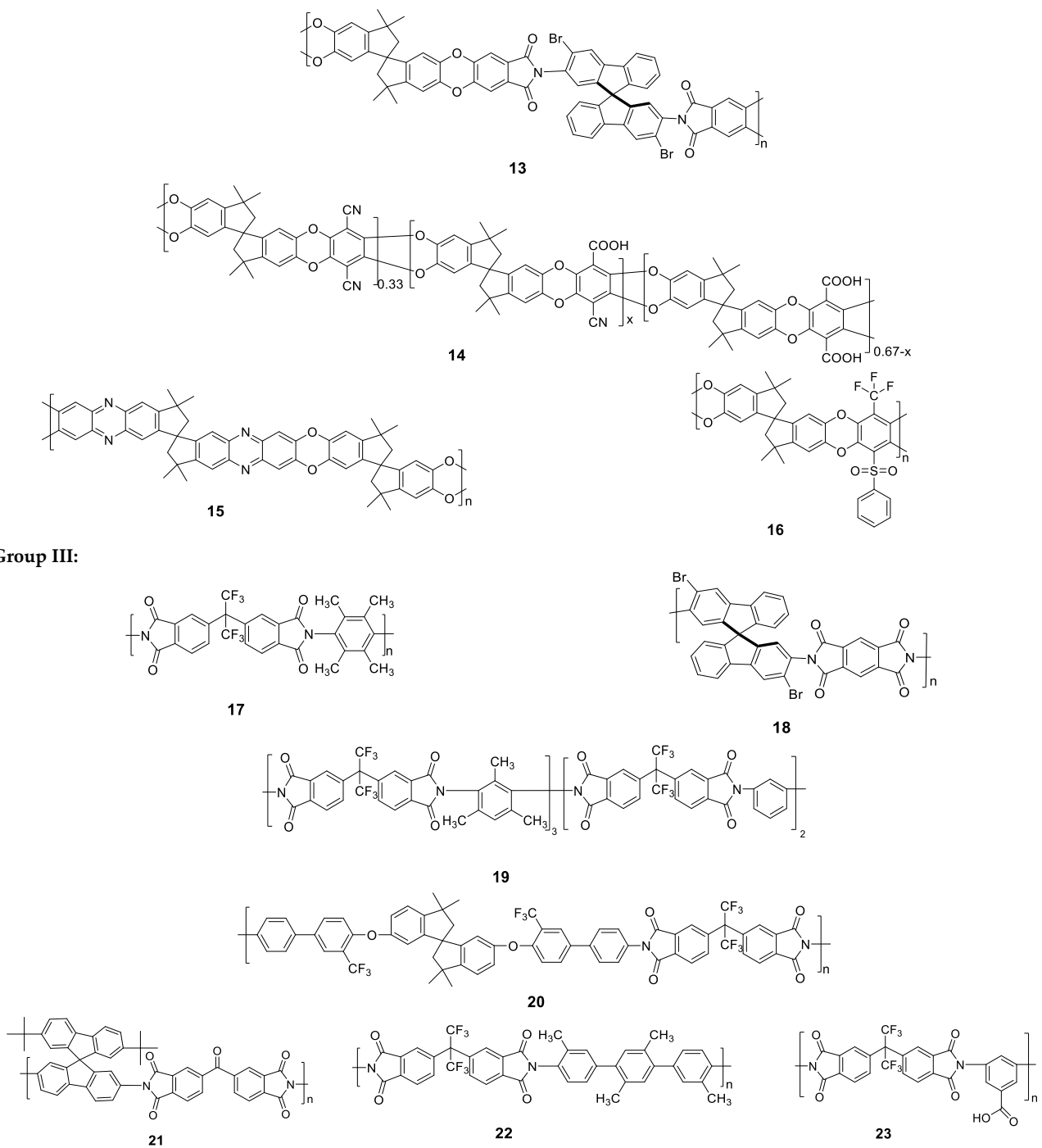


Chart 1. Chemical structures of membrane polymers in Figure 3 (All polymers until 2013).

2.1.1. Poly(Substituted Acetylene)s (PAs) (Group I: Polymers 1–9 in Chart 1 and Figure 3, and Polymers 24–34 in Chart 2 and Figure 4)

In the milestone paper which reported Robeson's 1991 upper bound line [10], it was described that glassy polymers generally show better performances than rubbery polymers. For example, poly (substituted acetylene)s (PAs) are typical glassy polymers with very high glass transition temperatures (T_g) because of their very rigid chemical structures created by their conjugated backbones with bulky and crowded side groups. In fact, PAs reported until 2013 show relatively good performance in oxygen permselectivity as shown in Figure 4 and Table 2 [36–43]. They are plotted at very close to or on Robeson's 1991 upper bound line but do not exceed the 2008 line until 2013.

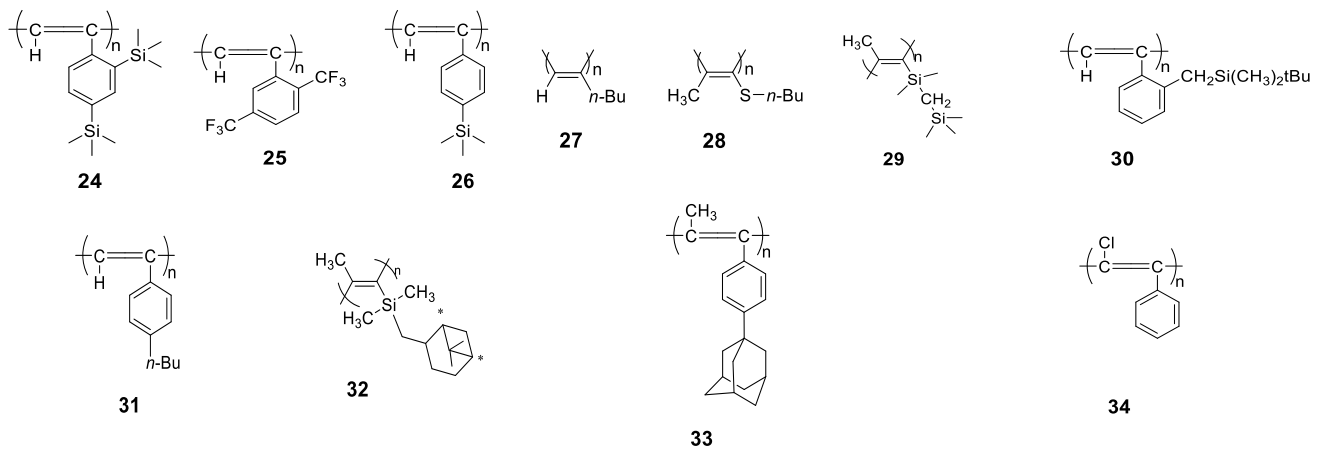


Chart 2. Chemical structures of the membrane polymers in Figure 4 (PAs until 2013). For 1–9, see Chart 1.

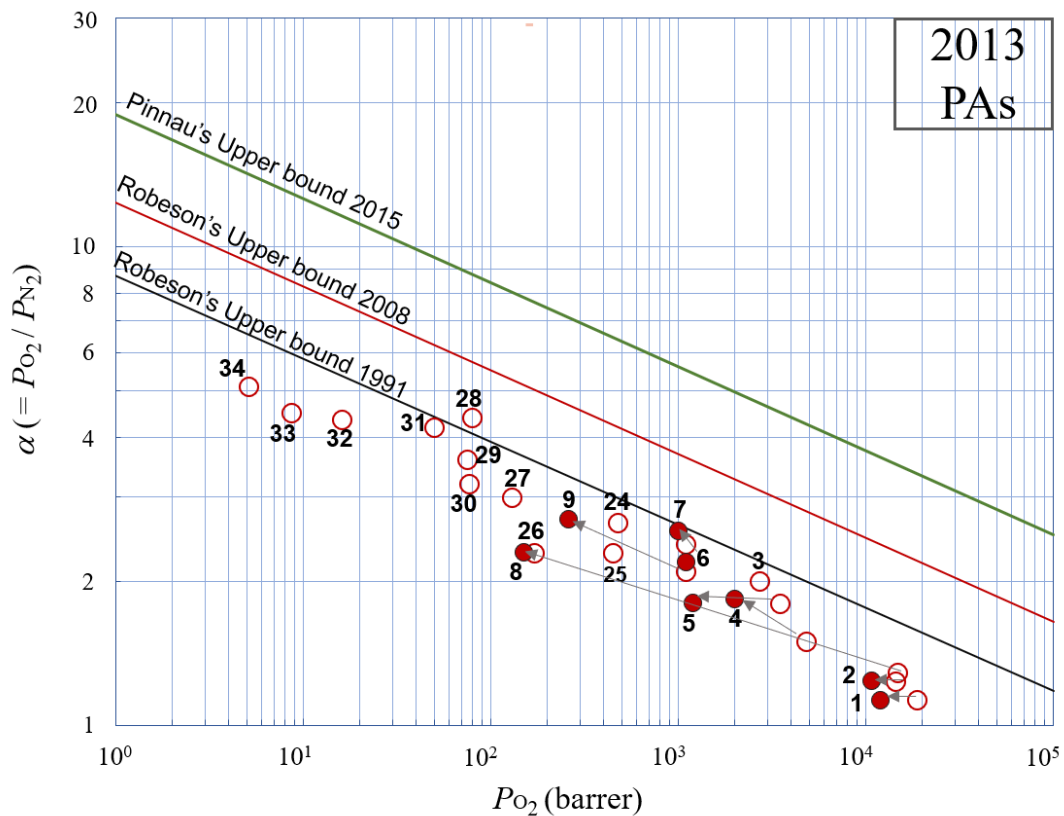


Figure 4. Plots of oxygen permselectivity through poly(substituted acetylenes) (PAs), showing the highest α at each P_{O_2} reported in the literature until 2013 (●: after aging, ○: before aging). For the data and categorization of the plots, see Table 2, and for the chemical structures of the polymers in the plots, see Charts 1 and 2.

Table 2. Categorization and detail data for the membrane polymers in Figure 4 (PAs until 2013).

Code	P_{O_2} (Barrer)	$\alpha (=P_{O_2}/P_{N_2})$	Thickness (μm)	Feed Gas	Ref. (Year)
24	(473)	(2.65)	-	mixed	[36] (1994)
25	(450)	(2.30)	30–100	mixed	[37] (1992)
26	(171)	(2.30)	-	mixed	[36] (1994)
27	(130)	(3.00)	10–100	pure	[38] (1988)
28	(79.0)	(4.40)	-	pure	[39] (1990)
29	(75.0)	(3.60)	10–100	pure	[38] (1988)

Table 2. Cont.

Code	P_{O_2} (Barrer)	$\alpha (=P_{O_2}/P_{N_2})$	Thickness (μm)	Feed Gas	Ref. (Year)
30	(77.0)	(3.20)	-	-	[40] (1995)
31	(50.0)	(4.20)	-	-	[41] (1998)
32	(16.0)	(4.35)	61.9–90.3	mixed	[42] (1996)
33	(8.60)	(4.50)	-	-	[43] (1999)
34	(5.10)	(5.10)	10–100	pure	[38] (1988)

[Note] For the codes, see Chart 2 and 1–9 are the same as those in Table 1. Data in parentheses are ones before aging.

Among the best 20 PAs, polymers 7 and 28 show the best and second-best performances, as shown in Figure 4. Polymer 7 lying on the 1991 upper bound line shows ultrahigh P_{O_2} around 10^3 with relatively high α [20]. This polymer has two trimethylsilyl and two phenyl groups. Polymers 9, 24, and 26 show lower P_{O_2} with similar α values compared with polymer 7. All these three polymers have one or two trimethylsilyl and two phenyl groups. Among these four PA type polymers, the polymer 7 from the monomer with the greatest number of trimethylsilyl and phenyl groups is the best. These bulky groups may create large amounts of micropores and the high mobility of the trimethylsilyl groups may maintain a high P_{O_2} . Polymer 28 show the best performance among the best 20 PAs [39]. Only this polymer includes polar atoms, sulfurs. The other nineteen polymers consist of only non-polar atoms, i.e., carbon, silicon, and hydrogen which do not induce polarity in the molecule. Therefore, it is thought the polar structure might enhance the α_S .

2.1.2. Poly(1-Trimethylsilylpropyne) (PTMSP) (an Ultraparpermeable Polymer) (Polymer 8 in Figures 3 and 4)

Among the PAs in Figure 4 (1–9 in Chart 1 and 24–34 in Chart 2), only a few PAs (1–7) show very high P_{O_2} values of more than 10^3 . The highest value is more than 10^4 . Such polymers are called ultraparpermeable polymers [44]. They are all poly(disubstituted acetylene)s (DPA). Poly(1-trimethylsilylpropyne) (PTMSP, polymer 8 in Chart 1) [45,46] reported by Prof. Masuda in 1983 is most meritorious among DPAs. The high P_{O_2} value (10^4) was much higher than that (10^2) for poly(dimethylsiloxane) (PDMS) which had been the highest value before his discovery. After this discovery, a great number of chemists, physicists, and materials scientists started new research projects concerning PTMSP in order to clarify the reason for the extremely high P_{O_2} value and to try to apply it to practical use. As a result, it was found that the extremely high P_{O_2} was caused by an unusually high fractional free volume (FFV, around 25–30%), which is also sometimes called ultrahigh FFV, or a large amount of very large micropores. The density is also the lowest (around 0.75). Therefore, the polymer is also called a super-glassy polymer. The sizes of the unusually large micropores in PTMSP have been reported in many papers as follows: 0.5–1.0 nm by Bakers [9], 0.9–1.2 nm by Robeson [12], 1.12 nm by Freeman [47], 1.24 nm by Lee [48], 1.1–1.5 nm by Pinnau [49], 0.45–0.55 nm by Yampolskii [50]. Judging from these reports, the sizes of the pores in PTMSP may be around 0.5–1.5 nm.

As described above, in order to separate oxygen (3.46 Å) and nitrogen (3.64 Å) based on the molecular sieving mechanism, pore sizes should be less than 1.0–0.5 nm. Since the sizes of the pores in PTMSP may be around 0.5–1.5 nm as described above, PTMSP is partially suitable for oxygen/nitrogen separation membranes on the basis of the MS mechanism. In fact, it was reported that the permselectivity $\alpha (P_{O_2}/P_{N_2})$ of PTMSP was mainly due to the diffusion selectivity, $\alpha_D (D_{O_2}/D_{N_2}) (=1.4)$ and no dissolution selectivity, $\alpha_S (S_{O_2}/S_{N_2}) (=1.1)$ was detected [9,51].

Although the P_{O_2} value of PTMSP is very high, the α value is extremely low, around 1.3. The pores in PTMSP whose sizes are around 0.5–1.5 nm are categorized both as micropores (<2.0 nm), useful for high P_{O_2} , and ultramicropores (<0.7 nm), useful for high α , but PTMSP contains mainly micropores and only a small amount of ultramicropores. Therefore, the P_{O_2} is very high and the α is very low. Another possible reason for the extremely low α value is the effect of partial permeation based on the Knudsen (Kd) mechanism. If the

permeation was solely based on the Kd mechanism, no dissolution selectivity should be found. Therefore, its α should be $\alpha_D = 0.93$. If the contribution of possible dissolution selectivity values is considered, the α values are 1.5–2.1 [12]. Since it was reported that the oxygen permeation behavior through PTMSP is within the transition range from SD mechanism to Kd mechanism [12], this possible reason may be reasonable.

A search of papers for P_{O_2} values for PTMSPs results in scattered values from 10^4 to 10^2 . This is unusual. Because a P_{O_2} value generally and inherently is one of physical properties of a usual polymer, the P_{O_2} should depend on the chemical structure of the polymer. Therefore, a polymer has its own specific P_{O_2} value. However, in general, the same polymers do not always produce the same homogeneous dense membranes because their high-order structures such as crystallinity, and their membrane structures, such as an asymmetric structure, are not the same in each case. In the case of PTMSP membranes that have a variety of P_{O_2} values, they can have quite different pore sizes. One of the reasons why the reported values of the pore sizes for PTMSPs were scattered as described above is that the sizes depend on the membrane preparation method. This variation of the pore sizes suggests instability of the micropores. In fact, strong aging effects were reported for the P_{O_2} values. The pore sizes must have been also decreasing with time. This may be another reason for the scattered data for the pore sizes. In fact, the very high P_{O_2} decreased significantly from 10^4 to 10^2 over time. The change is shown in Figures 3 and 4 (●: after aging, ○: before aging).

Although PTMSP and PDMS similarly show very high P_{O_2} values, the physical properties of PTMSP and PDMS are completely different and therefore their permeations are based on different permeation mechanisms. While PTMSP is a very rigid super-glassy polymer (whose T_g is thought to be more than 200 °C) with the lowest density, PDMS is a very flexible polymer with the lowest $T_g = -123$ °C. PTMSP has static micropores but PDMS has no micropores. As a result, permeation through PTMSP mainly follows the MS mechanism and permeation through PDMS follows the SD mechanism, although their performances are similar.

2.1.3. Poly(Diphenylacetylene)s (PDPAs) (Polymers 1, 2, 4–7, and 9 in Chart 1)

In Figure 4, there are some poly(substituted acetylene)s showing ultrapermeability, i.e., P_{O_2} of more than 10^3 even after aging (polymers 1–7), although PTMSP shows ultrapermeability only before aging. Most of them are poly(diphenylacetylene)s (PDPAs) (polymers 1–7, except for 3). PDPAs have a more rigid backbone than PAs in general because they have bulky substituted phenyl groups at every carbon of the main chain. Although they show very high P_{O_2} even after aging similar to non-aged PTMSP, their α values tend to be low and further from the upper line compared with other PAs. This may be caused by the permeation mechanism including not only the SD mechanism but also the Kd mechanism. In particular, the two PDPAs with indan groups (polymers 1 and 2) show extremely high P_{O_2} of more than 10^4 even after aging, similar to non-aged PTMSP. There are almost no aging effects on their performances, a situation quite different from PTMSP, as shown in Figure 3 (●: after aging, ○: before aging).

2.1.4. Spiro-PIMs (Polymers of Intrinsic Microporosity with Spirocarbons) (Group II: Polymers 10–16 in Figure 3 and Chart 1)

In the plots of the best polymers until 2013 (Figure 3), although the plots of the polymers showing high P_{O_2} of more than 10^3 (PDPAs) are below the 1991 upper bound line, the polymers (10–16) showing intermediate P_{O_2} values from 10^2 to 10^3 are located above the 1991 upper bound line. All these polymers are called PIMs (polymers of intrinsic microporosity) and related PIMs. Therefore, the new class of polymer contributed significantly to the appearance of the new improved 2008 upper line.

(1) Advent of the first PIM (PIM-1, 11 in Chart 1 and Figure 3)

The first PIM with an excellent P_{O_2} and α (11 in Chart 1 and Figure 3) was reported in the non-aged state by Budd and McKeown in 2005 [29]. Although network amorphous

polymers like carbon molecular sieve membranes (CMSMs) contain a large fractional free volume (FFV), they were insoluble and had no processability for their self-supporting membranes. Therefore, they designed a soluble non-network amorphous polymer containing a large FFV, called PIM-1 (no.11 in Figure 3). The new polymer is a linear macromolecule consisting of a very rigid fused rings backbone connected by spiro-carbons at contorted positions (In this review, this type of PIM is called Spiro-PIM). Because this is a linear (ladder) polymer, it is soluble and processable. In addition, the rigid ladder (fused rings) backbone with the kink points (spiro-carbons) can create relatively stable large micropores. As a result, it shows good performance beyond the 1991 upper line. The α for non-aged PIM-1 (11○ in Chart 1 and Figure 3) [25] is much higher than that for non-aged PTMSP (8○ in Chart 1 and Figure 3) [14], although the P_{O_2} for non-aged PIM-1 is much lower than that of PTMSP. The plot for PIM-1 lies above the 2008 upper bound after aging, although the P_{O_2} is less than 10^3 . It was reported that the selectivity of permeation ($\alpha = 2.8$) mainly depended on that of diffusion ($\alpha_D = 2.8$) and that of dissolution ($\alpha_S = 1.0$) was almost unity (no selectivity) suggesting it follows the MS mechanism [24]. This better α is because the size of pores, determined by nitrogen adsorption, in PIM-1 was much smaller (around 6.5 Å) than that (around 9 Å) in PTMSP [13].

(2) Improved Spiro-PIM (polymers 10 and 15 in Chart 1)

In addition, to enhance the rigidity of the main chain of PIM-1, a bulky group (fluorene) was introduced around the spirocarbons (10) or the fused rings backbone was extended (15). Compared with PIM-1 (11 in Chart 1 and Figure 3) both the P_{O_2} and α increased for PIM 10. This is because the introduction of the additional fused benzene rings restricted motion around the spiro-center of the backbone. The selectivity of permeation ($\alpha = 3.4$) mainly depended on that of diffusion ($\alpha_D = 3.4$) and that of dissolution ($\alpha_S = 1.0$) was almost unity (no selectivity) suggesting it follows the MS mechanism [24]. In the case of no.15 PIM, both the α and P_{O_2} decreased compared with no. 11. The lower ratio of the kink points may enhance the stacking of the backbones to reduce their micropores or FFV.

The two Spiro-PIMs (10 and 11 in Chart 1) described above showed strong aging effects as shown in Figure 3 (● and ○), similar to PTMSP (8). Therefore, several different α and P_{O_2} values were reported by different researchers. Both of the two PIMs lie above the 2008 upper bound after aging, although P_{O_2} values are less than 10^3 .

(3) Spiro-PIMs with side groups (modified Spiro-PIMs) (14 and 16 in Chart 1)

Side groups were introduced to Spiro-PIMs (14 and 16). Compared with PIM-1 (11), both α and P_{O_2} decreased. The polar groups may enhance intermolecular interactions to reduce their micropores or FFV.

(4) Spiro-PIM-PI (12 and 13 in Chart 1)

The other related PIMs that are plotted above the 1991 upper bound line are new PIMs which include imido-structures (Spiro-PIM-PI, 12 and 13). However, compared with PIM-1 (11), their performances are not superior. Introducing the simple single bonds of C–N into the PIMs' ladder backbones may reduce the rigidity which is effective for good performance. However, compared with usual polyimides describe below, they have higher P_{O_2} values.

2.1.5. Polyimides (PIs) (Group III: 17–23 in Chart 1 and Figure 3, and 35–43 in Chart 3 and Figure 5)

In Figure 3 for all the best polymers until 2013, polymers 17–23 show high α values and low P_{O_2} values. They are all polyimides (PIs). Among them, polymers 20 and 21 show the top two highest α values. They contain contorted backbones. Therefore, they are also categorized as Spiro-PIM-PI as mentioned above.

Figure 5 shows plots of the best PIs until 2013. Table 3 lists the detailed data for the polymers in Figure 5 [52–54]. They are amorphous and have very high Tg values, that is, they are glassy polymers. Conventional PIs are known as insoluble polymers

and, therefore, they have no direct processability and their membranes are prepared from their soluble precursor polymers called poly(amic acid)s [55]. However, by introducing bis(trifluoromethyl)methylene ($-(CF_3)_2C-$) to the main chain of PIs, they became soluble and therefore direct fabrication to their membranes became possible. The bulky groups inhibit efficient packing of the polymer chains resulting in higher permeability. In fact, almost all the PIs showing the best performances here in Figure 5 include the fluorine-containing group ($-(CF_3)_2C-$), except for polymers 40 and 43 and PIM-PIs (35, 36, 18, 20, and 21) (Charts 1 and 3). The PIs can be classified into two groups. One group contains a lot of methyl groups (polymers 17, 19, 22, 37–44) and the other have contorted spiro carbons (polymers 18, 20, 21, 35, and 36; PIM-PI, the details are described above). The PIs with many methyl groups (39, 19, 41, 22) had relatively high densities around 1.3–1.4 and low FFVs of about 10–20%. However, they had relatively large spaces between macromolecules, because their d -spacing values from XRD were 0.46–0.57 nm [56] and their pore sizes by PALS [48] were 0.6–0.7 nm. In other words, these PIs may contain ultramicropores (<0.7 nm). It was reported that their selectivities of permeation (α) through these PIs mainly depended on those of diffusion (α_D) and those of dissolution (α_S) were almost unity (<1.2) [32,52]. Therefore, since the permeation may involve the MS mechanism, relatively high α values are shown. However, since they have no large micropores (0.7–1.0 nm), unlike PTMSP, their P_{O_2} values were low.

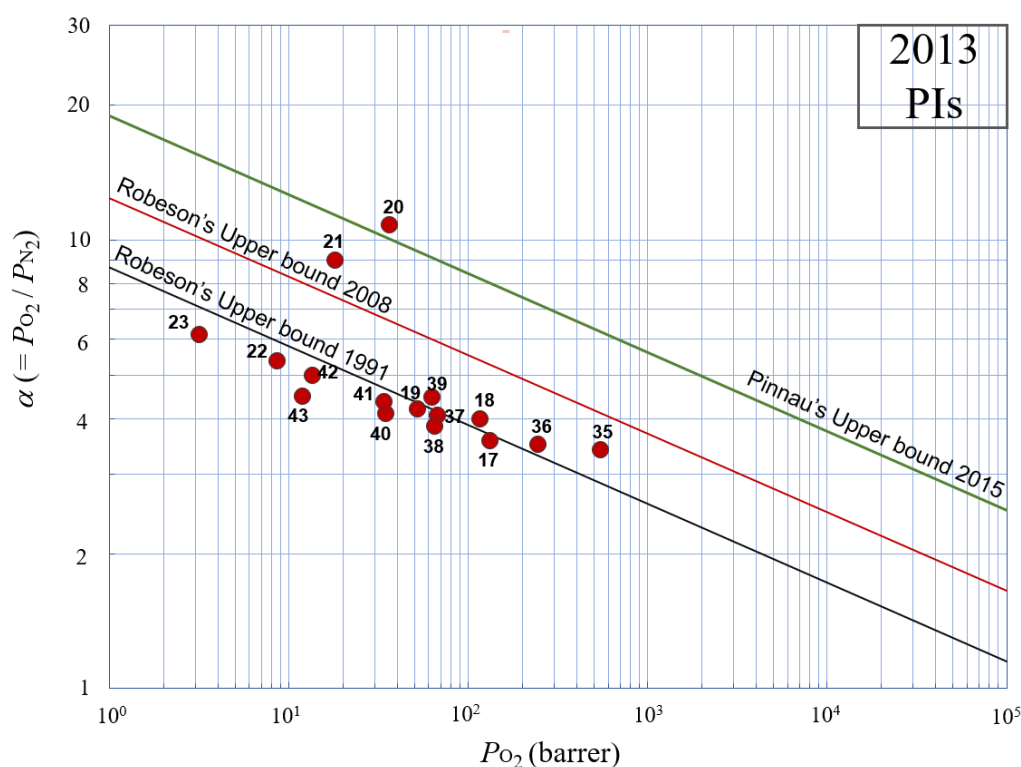
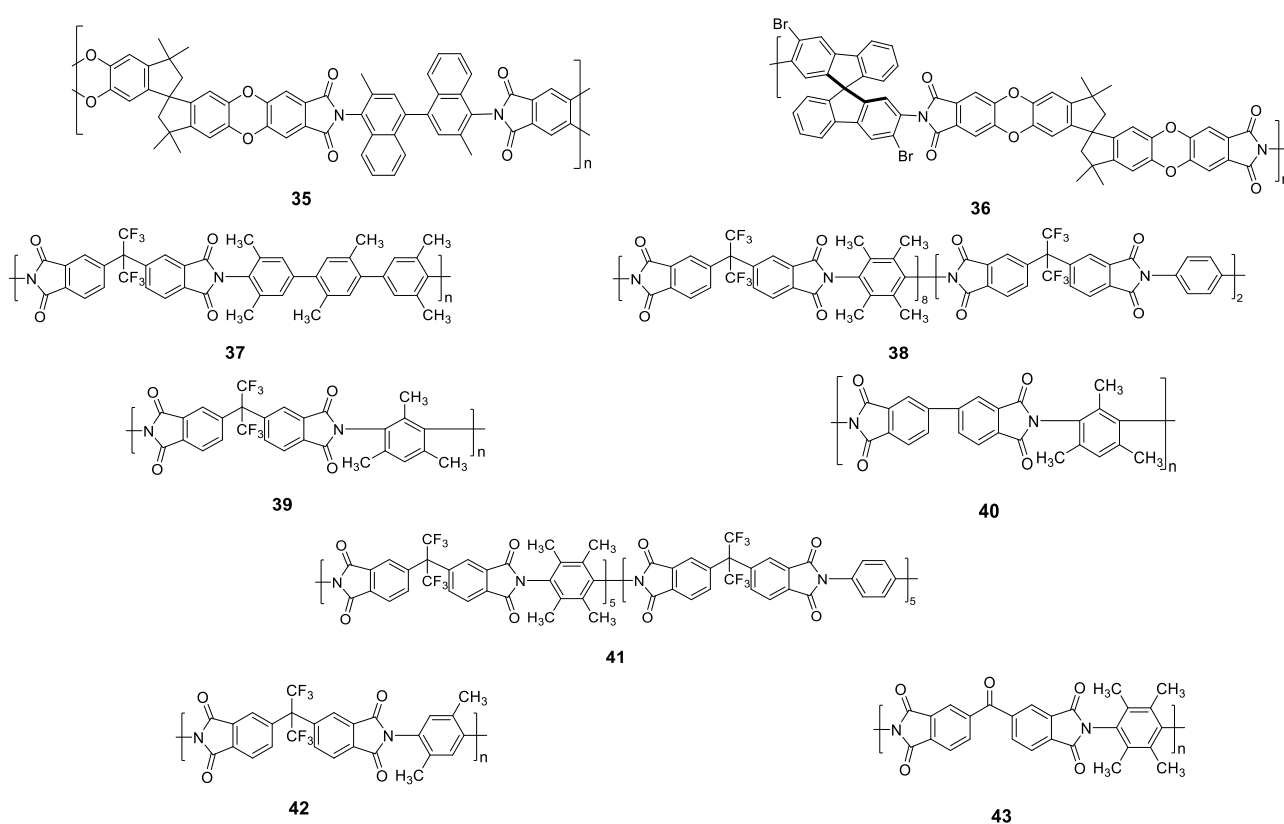


Figure 5. Plots of oxygen permselectivity through polyimides (PIs), showing the highest α at each P_{O_2} reported in the literature until 2013. For the data and categorization of the plots, see Table 3, and for the chemical structures of the polymers in the plots, see Charts 1 and 3.

Table 3. Categorization and detail data for the membrane polymers in **Figure 5** (PIs until 2013).

Code	P_{O_2} (Barrer)	$\alpha (=P_{O_2}/P_{N_2})$	Thickness (μm)	Feed Gas	Ref. (Year)
35	545	3.40	96	pure	[26] (2008)
36	243	3.50	80–100	pure	[27] (2013)
37	67.0	4.06	30–90	pure	[35] (1999)
38	64.8	3.84	-	pure	[52] (2000)
39	62.5	4.46	30	mixed	[53] (1999)
40	34.7	4.10	-	mixed	[54] (1992)
41	33.8	4.37	-	pure	[52] (2000)
42	13.4	5.00	-	mixed	[54] (1992)
43	11.8	4.48	30	mixed	[53] (1999)

[Note] For the codes, see Chart 3.

**Chart 3.** Chemical structures of the membrane polymers in **Figure 5** (PIs until 2013). For 17–23, see **Chart 1**.

2.2. Top-Performing Polymers in 2020 as Oxygen/Nitrogen Permselective Membranes

After we had reviewed the data until 2013 and summarized them as described in 2.1, we then thoroughly searched for reports published from 2014 to the present and renewed the plots for top-performing polymers from the previous plots until 2013 (**Figure 3**) to the latest plots (**Figure 6**) of polymers showing the highest α at each P_{O_2} reported until 2020. The values and categorization are listed in **Table 4** [57–69]. The chemical structures of these polymers showing the best performances are shown in **Chart 4**. It is very surprising that many high-performance polymers which are beyond the 2008 upper bound line appeared in this period of 2014–the present. It is very clear that the progress is very rapid by comparing the changes for six years in 2014–2020 in **Figure 6** with those for the 22 years 1991–2013 in **Figure 3** (The plots in **Figure 3** are also shown by open small circles with thin lines in **Figure 6**).

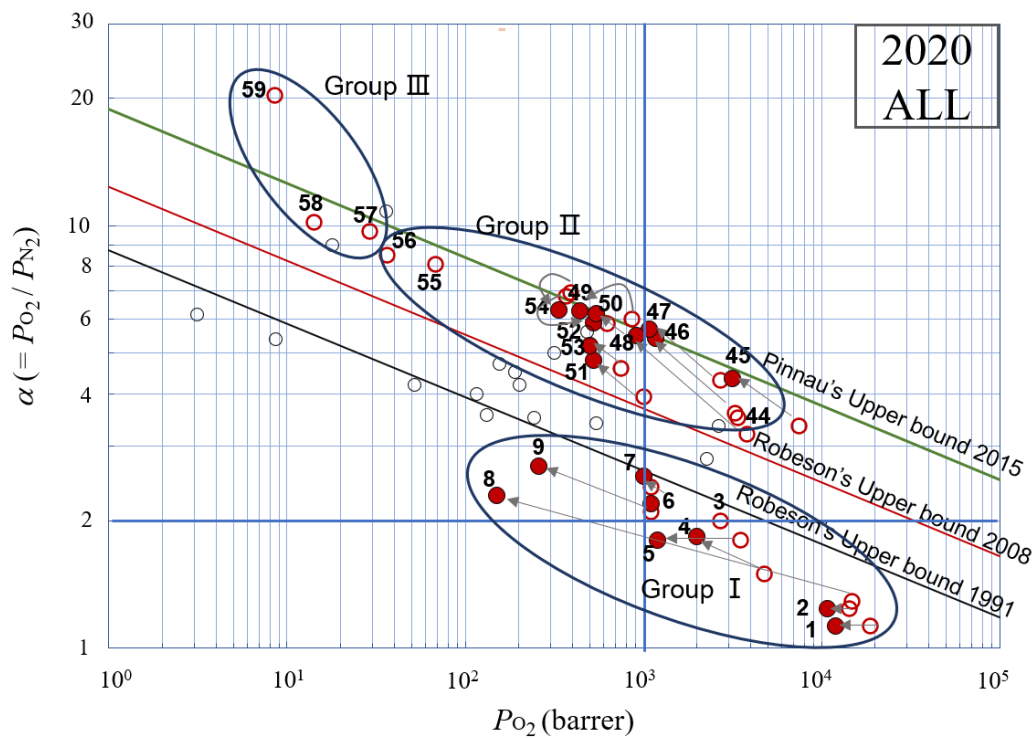


Figure 6. Plots of oxygen permselectivity through polymers, showing the highest α at each P_{O_2} reported in the literature in 2020 (●: after aging, ○: before aging). For the data and categorization of the plots, see Table 4, and for the chemical structures of the polymers in the plots, see Charts 1 and 4. The small open circles indicate data in Figure 3. [Note] Please compare this figure with Figure 3. You can recognize a big advance between 2013–2020 and also no advance of polymers in Group I.

Table 4. Categorization and detailed data for the membrane polymers in Figure 6 (all polymers in 2020).

Code	Polymer Type	P_{O_2} (Barrer)	α ($=P_{O_2}/P_{N_2}$)	Thickness (μm)	Casting Solvent	Feed Gas	Aging Time (Days)	Ref. (Year)
Group I (see Table 1)								
Group II								
44	Spiro-PIM	(3410)	(3.50)	-	chloroform	pure	-	[57] (2016)
45	Trip-PIM	3160 (7470)	4.35 (3.35)	187 (195)	-	pure	365	[44] (2017)
46	Trip-PIM	1170 (3290)	5.40 (3.60)	180	chloroform	pure	166	[58] (2015)
47	Trip-PIM	1073 (2718)	5.70 (4.30)	132	chloroform	pure	100	[59] (2014)
48	Spiro-PIM	910 (3820)	5.50 (3.20)	115	chloroform	pure	1295	[23] (2018)
49	Trip-PIM	440 (864)	6.29 (6.01)	60	chloroform	pure	150	[60] (2020)
50	Trip-PIM-PI	542 (627)	6.20 (5.86)	77	chloroform	pure	150	[61] (2014)
51	Ladder	528 (747)	4.80 (4.60)	39	chloroform	pure	300	[62] (2020)
52	Trip-PIM	525 (368)	5.90 (6.80)	-	chloroform	pure	15	[44] (2017) [63] (2014)
53	Trip-PIM	500 (1002)	5.21 (3.93)	-	chloroform	pure	407	[64] (2020)
54	Trip-PIM	334 (374)	6.30 (6.93)	-	chloroform	pure	150	[60] (2020)
55	Trip-PBO	(68)	(8.10)	-	DMAc	pure	-	[65] (2018)
56	Ladder	(36.5)	(8.50)	45	chloroform	pure	-	[66] (2017)

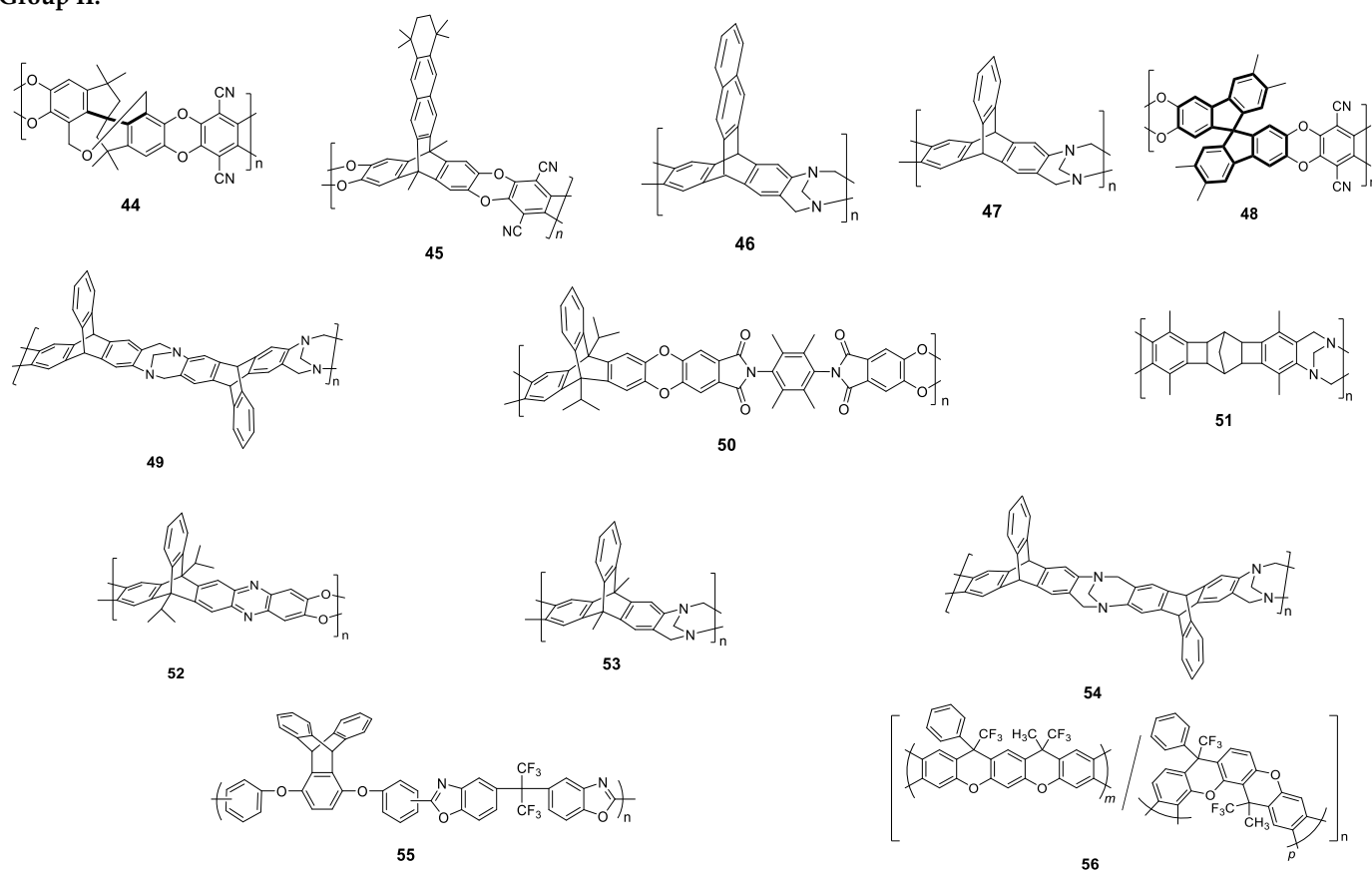
Table 4. Cont.

Code	Polymer Type	P_{O_2} (Barrer)	α ($=P_{O_2}/P_{N_2}$)	Thickness (μm)	Casting Solvent	Feed Gas	Aging Time (Days)	Ref. (Year)
Group III								
57	PAm	(29.0)	(9.67)	70–80	DMAc	pure	-	[67] (2015)
58	PAm	(14.2)	(10.2)	70–80	DMAc	pure	-	[68] (2015)
59	PI	(8.52)	(20.3)	65–75	DMF	pure	-	[69] (2016)

[Note] For the codes, see Chart 4. Data in parentheses are ones before aging.

Group I: For 1–9, see Chart 1.

Group II:



Group III:

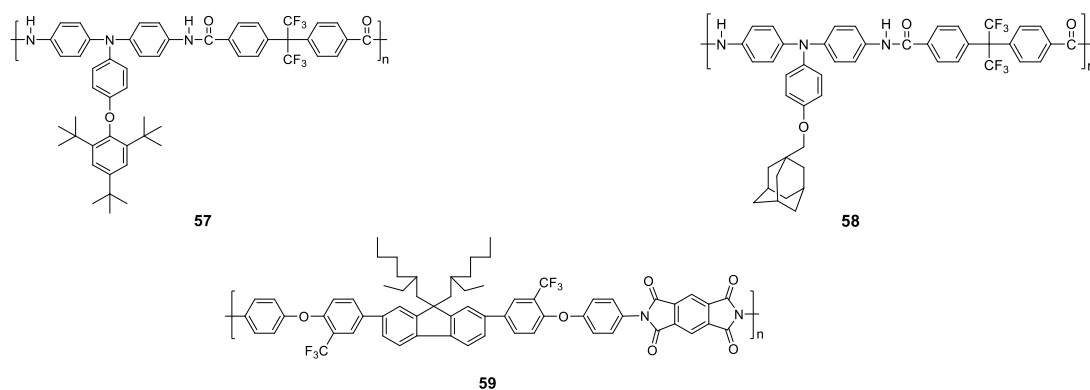


Chart 4. Chemical structures of the membrane polymers in Figure 6 (all polymers in 2020).

The polymers can be categorized into the following three groups. Group I: polymers 1–9 (Chart 1) with the highest P_{O_2} and the lowest α below the 1991 upper bound line, Group II: polymers 44–56 (Chart 4) with high α and high P_{O_2} beyond the 2008 upper

bound line and close to, or on, the 2015 upper bound line, and Group III: polymers 57–59 (Chart 4) with the highest α and the lowest P_{O_2} beyond the 2008 upper line and close to, or beyond, the 2015 upper bound line. Typical polymers categorized into Groups I, II, and III are poly (disubstituted acetylenes) such as poly (1-trimethylsilylpropyne) (PTMSP) and poly(diphenylacetylene)(PDPA), ladder polymers with side arylene groups without spirocarbons (Trip-PIM), and polyamides (PAm) or polyimide (PI) with bulky pendant groups, respectively. The details are described below.

2.2.1. Poly(diphenylacetylene)s (PDPAs) and Modified PAs (Group I; 1–9 in Figure 6 and Chart 1)

(1) Poly(diphenylacetylene)s (PDPAs)

In the plots of this region in Figure 6 (polymers 1–9 in Chart 1), the situation is similar to that until 2013 (Figure 3, polymers 1–9). Therefore, no noticeable improvements in this region have occurred in the period since 2014 to the present (for the discussion, see Section 2.1.3).

(2) Modified PAs (60–78 in Figure 7 and Chart 5;)

Table 5. Categorization and detailed data for the membrane polymers in Figure 7 (PAs in 2020).

Code	Polymer Type (Subcategory of PA)	P_{O_2} (Barrer)	$\alpha (=P_{O_2}/P_{N_2})$	Thickness (μm)	Casting Solvent	Feed Gas	Ref. (Year)
1	DPA	12,000 (18,700)	1.13 (1.13)	80–120	toluene	pure	[14] (2008)
2	DPA	10,800 (14,400)	1.24 (1.24)	-	toluene	pure	[15] (2008)
4	DPA	2000 (4800)	1.84 (1.43)	80	toluene	pure	[17] (2009)
5	DPA	1200 (3500)	1.80 (1.80)	-	toluene	pure	[18] (2006)
7	DPA	1000 (1100)	2.55 (2.40)	30–120	-	mixed	[21] (1993) [14] (2008)
8	DPA (PTMSP)	150 (14,800)	2.30 (1.29)	-	cyclohexane	pure	[22] (1992)
9	DPA	260 (1100)	2.70 (2.10)	-	-	pure	[21] (1993)
60	2DP networked (blend)	(5320)	(2.45)	30–150	tetrahydrofuran	mixed	[70] (2019)
61	c-c PA (networked)	(1800)	(2.57)				
62	c-c PA (networked)	(4500)	(2.56)	40–100	chloroform	mixed	[71] (2018)
63	c-c PA (networked)	(6950)	(2.44)				
64	DPA	(3100)	(1.82)	50–80	toluene	pure	[72] (2014)
65	DPA	(1400)	(2.00)	140–200	toluene	pure	[73] (2017)
66	c-c PA	(1740)	(2.54)				
67	c-c PA	(1090)	(2.83)	30–50	chloroform	mixed	[74] (2018)
68	c-c PA	(405)	(3.00)				
69	c-c PA (networked)	(224)	(4.39)	30–120	tetrahydrofuran	mixed	[75] (2020)
70	2DP (networked) (calcd)	(341)	(4.24)				
71	c-t PA (networked)	(155)	(4.64)	30–120	toluene	mixed	[76] (2020)
72	c-t PA (networked)	(141)	(4.92)				
73	c-t PA (hyperbranched)	(112)	(4.38)	60–120	toluene	mixed	[77] (2017)
74	c-t PA (hyperbranched)	(106)	(4.46)				
75	c-t PA (hyperbranched)	(58.7)	(5.00)				
76	c-c PA (multi-stranded)	(101)	(3.68)	20	toluene	mixed	[78] (2017)
77	c-c PA (networked)	(5.00)	(6.35)	-	-	mixed	[70] (2019)
78	DPA	(4.00)	(8.90)	-	-	pure	[79] (2015)

[Note] For the codes, see Chart 5. The two polymers (3 and 6) are removed from the nine polymers (1–9) in Table 2, because the aged data for the two polymers were not reported until 2020. Data in parentheses are those before aging.

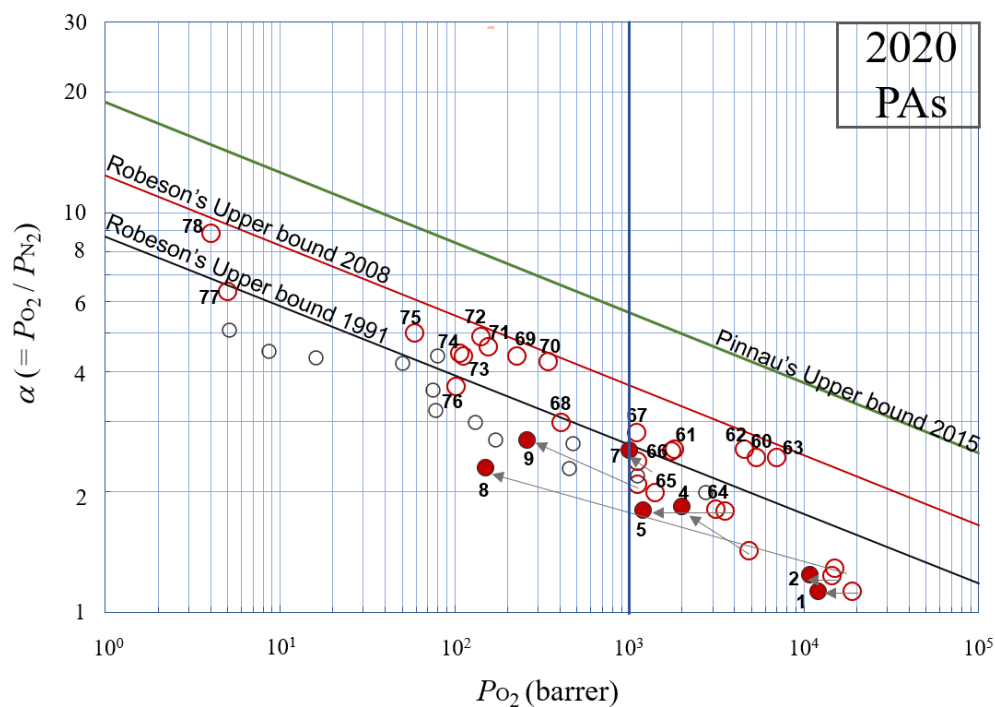


Figure 7. Plots of oxygen permselectivity through polyacetylenes (PAs), showing the highest α at each P_{O_2} reported in the literature in 2020 (●: after aging, ○: before aging). For the data and categorization of the plots, see Table 5, and for the chemical structures of the polymers in the plots, see Charts 1 and 5.

Figure 7 shows plots of all the PAs having good performance reported from 2014 to the present. The detailed data are listed in Table 5 [70–79]. Although until 2013, all the plots for PAs were below the 1991 upper bound line as shown in Figure 4 (the plots in Figure 4 are also shown by open small circles with thin lines in Figure 7), some of the plots for PAs in 2020 are located above the 1991 upper bound line and close to the 2008 upper bound line. Such developments have been realized using several methods by the author's group. The methods are categorized into the following three main groups. Category A: changing to more rigid cis-cis main chains in PAs than cis-trans PAs together with introducing soft linear siloxane side groups (c-c PAs and their derivatives; polymers 61–63, 66–68, and 76, 77 in Chart 5); Category B: introducing hyperbranched or soft crosslinked structures (network structures) into cis-trans PAs (c-t PAs and their derivatives; 71–75 in Chart 5); Category C: membranes containing network two-dimensional (2D) polymers derived from cis-cis PAs (c-t PAs and their SCAT (highly selective photocyclic aromatization) derivatives; 60 and 70 in Chart 5). In category A, since cis-cisoid polyphenylacetylenes (c-c PAs) are more rigid than c-t PAs and similarly to PDPAs, some c-c PAs show better performance than c-t PAs. In particular, a combination of the rigid backbone and soft and short oligosiloxane grafts are suitable (66) [74]. Introduction of soft crosslinking and modification by SCAT reaction of these types of polymer enhanced their performances (61–63) [71]. In category B, introducing hyperbranched (73–75) [77] or soft network (71 and 72) [76] structures to c-t PAs enhanced their permselectivities. In category C, by embedding two-dimensional (2D) polymers created by SCAT reaction of c-c PAs to membranes, good performances were realized. The 2DP 70 [75] was synthesized by interfacial polycondensation at the solid–solid interface and 2DP 60 membrane [70] was prepared by blending with polymer 9. In summary, it was found that a rigid backbone based on c-c PAs, soft short side chains and network structures including hyperbranched and 2DP structures were effective for enhancement of α values. Rigidification of PA's main chain enhanced α and P_{O_2} simultaneously (66) [74]. However, network structures (69, 71, 72, and 77) including a multi-stranded structure (76) [78] caused a decrease of P_{O_2} compared with the precursor linear polymers, although α increased. Only

in the cases of hyperbranched (73–75) [77] and 2DP structures (60 [70] and 70 [75]), was P_{O_2} also maintained.

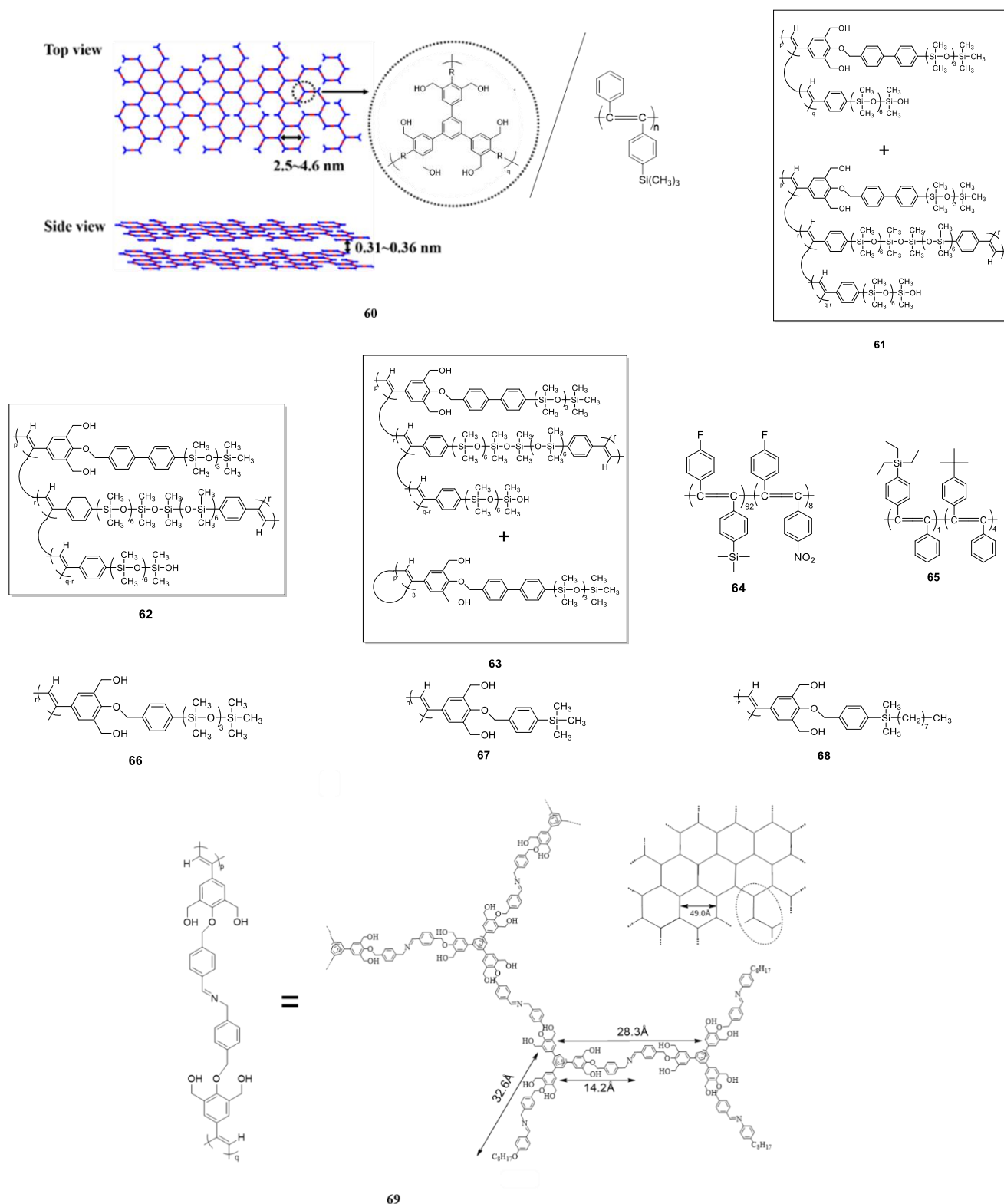
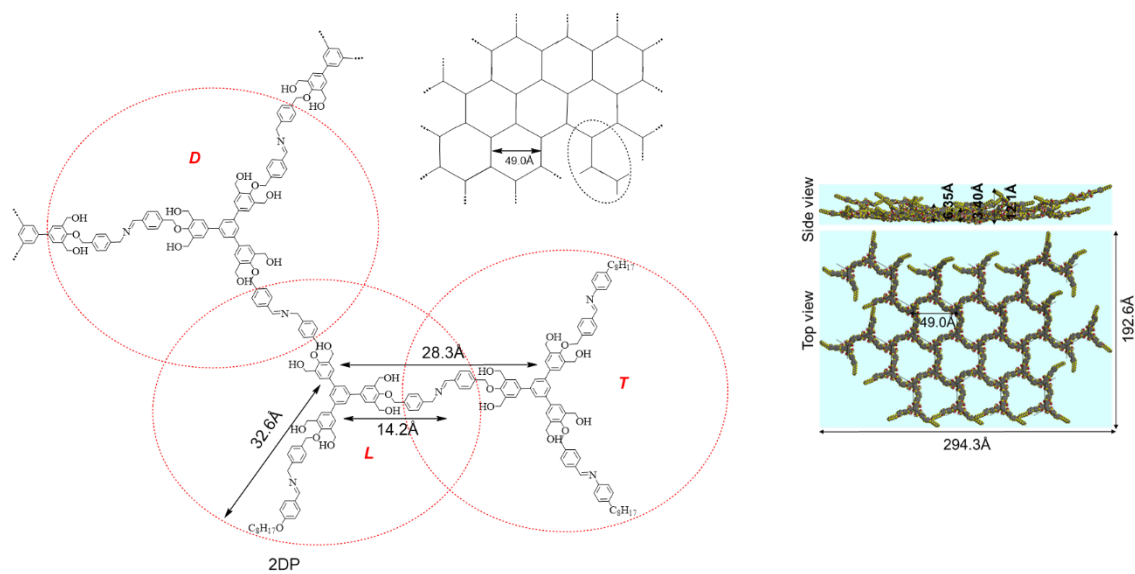
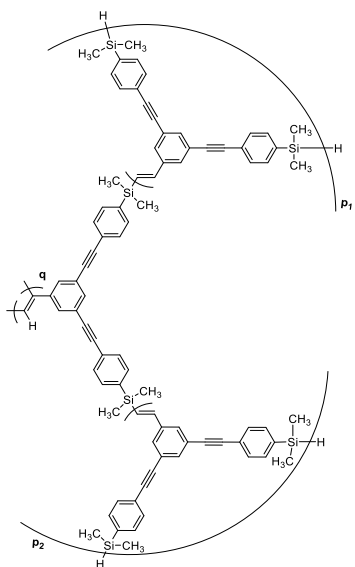
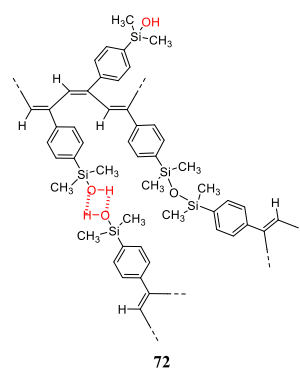
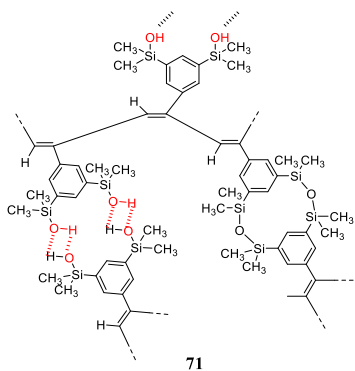


Chart 5. Cont.



70



73 (p/q = 1.69)
 74 (p/q = 1.75)
 75 (p/q = 2.75)

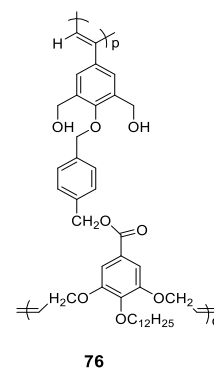


Chart 5. Cont.

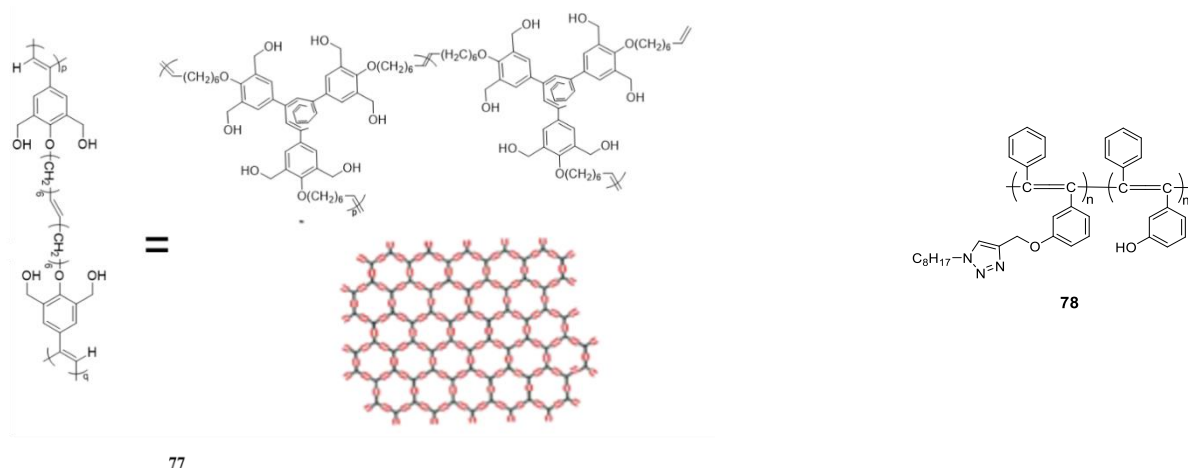


Chart 5. Chemical structures of the membrane polymers in Figure 7 (PAs in 2020). For 1–9, see Chart 1.

2.2.2. Ladder Polymers with Side Arylene Groups without Spirocarbons and Other Ladder Polymers (Group II; Polymers 44–56 in Figure 6 and Chart 4)

(1) Ladder polymers with side arylene groups without spirocarbons (Trip-PIMs)

As shown in Figure 6 for all the polymers until 2020, great developments are observed in the region between 10^2 and 10^3 (ultrapermeable region) of P_{O_2} compared with all the polymers until 2013 shown in Figure 3. They (44–56) are located above the 2008 upper bound line and in particular some of the polymers (45–50, 52, and 54) are located far above the 2008 upper bound line. Pinnau's 2015 upper bound line [13] was newly drawn because the three polymers (47, 50, and 52) appeared in 2014. Most of them (except for 44 and 51) are a new type of PIM having rigid ladder backbones similar to Spiro-PIM. However, the new PIMs contain no spirocarbons in their main chains and instead they contain triptycene (Trip) groups as kink points in their backbones. Therefore, in this review they are called Trip-PIM. By contrast with Spiro-PIMs described in Section 2.1.4, the backbones of Trip-PIMs have totally ladder structures.

Although the three polymers reported in 2014 (47, 50, and 52) made a significant contribution to the new 2015 upper bound line [13], their P_{O_2} values were much less than 10^3 (ultrapermeable region) and lower than that for PTMSP (8 in Chart 1) (as described above, non-aged PTMSP has a large amount of micropores around 13 Å which is effective for the very high P_{O_2} .) These excellent performances of Trip-PIMs were caused by the effective size distribution of ultra-micropores (<7 Å) and micropores (<20 Å). For example, in the case of Trip-PIM 52, the sizes of ultramicropores [27] are smaller (around 5.3 Å) than those of Spiro-PIM (PIM-1) (around 6–7 Å) [13,27]. In addition, both the PIMs have similar amounts of a larger size of micropores (around 13 Å) useful for high permeability. Therefore, this Trip-PIM shows much better performance than the Spiro-PIM(PIM-1). Table 6 summarizes data of α (P_{O_2}/P_{N_2}), α_S (S_{O_2}/S_{N_2}), and α_D (D_{O_2}/D_{N_2}) values for some of Trip-PIMs (46, 47, and 53) plotted in Figure 6. For these polymers, the high α values depend only on α_D and their α_S values were around unity.

Table 6. Fractional free volume (FFV) and diffusion and dissolution selectivities for selected polymers.

Code	Polymer Type	P_{O_2} (Barrer)	FFV	α (P_{O_2}/P_{N_2})	α_D (D_{O_2}/D_{N_2})	α_S (S_{O_2}/S_{N_2})	Ref. (Year)
8	PA (PTMSP)	4860	0.340	1.60	1.47	1.06	[9] (1995)
11	Spiro-PIM (PIM-1)	317 (2270)	0.26 [30]	5.00 (2.80)	2.80	1.00	[25] (2015) [24] (2012)
45	Trip-PIM	3160 (7470)	0.309	4.35 (3.35)	-	-	[44] (2017)
46	Trip-PIM	1170 (3290)	-	5.40 (3.60)	4.70 (5.00)	1.14 (0.71)	[58] (2015)

Table 6. Cont.

Code	Polymer Type	P_{O_2} (Barrer)	FFV	α (P_{O_2}/P_{N_2})	α_D (D_{O_2}/D_{N_2})	α_S (S_{O_2}/S_{N_2})	Ref. (Year)
47	Trip-PIM	1073 (2718)	-	5.70 (4.30)	5.20 (3.40)	1.10 (1.26)	[59] (2014)
50	Trip-PIM-PI	542 (627)	-	6.20 (5.86)	- (5.06)	- (1.16)	[61] (2014)
52	Trip-PIM	525 (368)	-	5.90 (6.80)	- (6.58)	- (1.03)	[44] (2017) [63] (2014)
53	Trip-PIM	500 (1002)	-	5.21 (3.93)	5.01 (4.24)	1.04 (0.95)	[64] (2020)
55	Trip-PBO	(68.0)	-	8.10	6.75	1.18	[65] (2018)
57	PAm	(29.0)	0.188	9.67	3.88	2.47	[67] (2015)
58	PAm	(14.2)	0.159	10.2	4.67	2.19	[68] (2015)
59	PI	(8.52)	0.122	20.3	7.11	2.85	[69] (2016)

[Note] For the codes, see Charts 1 and 4. Data in parentheses are ones before aging.

Some substituent effects on the performances of Trip-PIMs were examined. The size of arylene groups as the side groups and the size or shape of alkyl groups at the bridge heads were changed. When the phenylenes (47 in Figure 6) [59] are changed to larger naphthylenes (46) [58], the P_{O_2} increases and α decreases. These α rely almost exclusively on α_D as shown in Table 6. The spaces may be enlarged by enhancing the size of the substituents. The bulkier substituents may create micropores suitable for P_{O_2} enhancement. On the other hand, when the alkyl groups at the bridge heads are changed from hydrogen groups (=no substituent, 47) ([59]) to bigger methyl groups (53), ref. [64] both P_{O_2} and α decrease at the same time. The small substituents may fill the original micropores. When the alkyl groups at the bridge heads were changed from *n*-propyl groups ($P_{O_2} = 101$, $\alpha = 5.7$ [63]) to *iso*-propyl groups (52), ref. [63] both P_{O_2} and α increased. These α values were almost exclusively on α_D as shown in Table 6. The rigidity may be increased by enhancing the bulkiness of the substituents and, therefore, ultramicropores suitable for α enhancement may form. In fact, the pore sizes were found to become narrower based on NLDFT analysis.

Among Trip-PIMs 47, 49, and 54 (Figure 6 and Chart 4) which are isomers to one another, and are all composed of triptycenes and Tröger's bases, polymer 54 shows the best α . The main chain of polymer 54 is relatively straight, while the others are not straight. Therefore, polymer 54 may create the smallest micropores among the three. Actually, polymer 54 has the highest density (0.931), lowest FFV (0.349), and smallest pore sizes (5.7 Å) [60].

Recently among Trip-PIMs, a new polymer (45) was reported to have extremely high P_{O_2} of more than 10^3 , i.e., ultrapermeability while maintaining their excellent α values (>4). This is the best performance up to the present [44]. This Trip-PIM has a totally complete ladder backbone having no Tröger's base units. In addition to the fact that Trip-PIMs have generally smaller ultramicropores than Spiro-PIMs as described above, this Trip-PIM also has a much higher population of larger micropores (7–10 Å) effective for enhancing P_{O_2} than a Spiro-PIM. Therefore, polymer 45 shows the best performance having both ultrahigh P_{O_2} and high α values. In fact, the FFV is very large (0.309), similar to PTMSP (Table 6).

(2) PIs with Trip

Polymer 50 showing one of the best performances is a polyimide containing Trip units. Several Trip-PIM-PIs were synthesized from different diamines [53]. Among them, polymer 50 showed the best performance. Because it contains tetramethylphenylene units, the rigidity of the C–N bonds may be the highest.

(3) Other ladder polymers

Two novel ladder polymers with no Trip groups and spiro carbons in their backbones (51 and 56) were reported as some of the best performance polymers. While Trip-PIMs are totally straight ladder structures with bulky side groups (1,2-phenylene groups), these new ladder polymers have no bulky side groups like a Trip. Since their ladder backbones

are not straight instead, they may have micropores. However, their performances are inferior to Trip-PIMs. Similar to the Trip-PIMs containing Tröger's base units (47, 49, and 54) mentioned above, the ladder polymer 51 containing Tröger's base units showed a similar tendency. The pure isomer polymer had a higher α and lower P_{O_2} .

(4) Modified Spiro-PIMs

The polymers 44 [57] and 48 [23] are modified Spiro-PIMs. The former polymer has a more rigid backbone made by introducing additional cyclic structure around the relatively flexible spirocarbons. In other words, this is a locked PIM-1 (11 in Chart 1). As a result, both P_{O_2} and α values are increased simultaneously. This may be caused by increasing the rigidity producing a longer interchain distance. The latter BenzoSpiro-PIM (48) with four methyl groups shows higher P_{O_2} and lower α than the original BenzoSpiro-PIM (10 in Chart 1 and Figure 3) without substituents.

Figure 8 summarizes the performance and progress of all the PIMs, that is, Spiro-PIMs and Trip-PIMs. It shows clearly that both P_{O_2} and α values are improved by a change from Spiro- to Trip-PIMs. In addition, they show a large decrease in P_{O_2} by aging. As a consequence, most aged PIMs are not ultrapermeable, except for polymers 45–47. However, plots for most of Trip-PIMs are located on the 2015 upper bound line at the aged state.

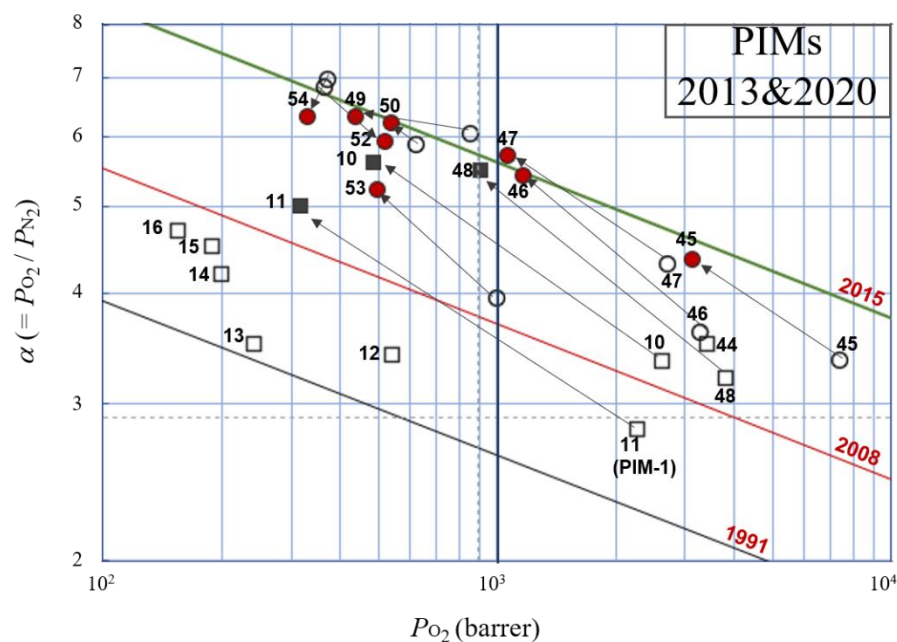


Figure 8. Plots of oxygen permselectivity through polymers of intrinsic porosities (PIMs), showing the highest α at each P_{O_2} reported in the literature until 2013 and 2020. For the numbers see Chart 1 (2013) and Chart 4 (2020). \bullet : Trip-PIM, \blacksquare : Spiro-PIM, \bullet : aged values, \square : none-aged values.

2.2.3. PI or Polyamides (PAMs) with Bulky Side Groups (Group III, 57–59 in Figure 6 and Chart 4)

As described in 2.1.5, the polyimide (PI) (20 reported in 2010 in Chart 1 and Figure 3 until 2013) shows an unusually high α value (10.8). In this case, kink points were introduced to a PI by spirocarbon structures in a similar way to Spiro-PIMs. In Figure 6 in 2020, some condensation polymers of not only PI (59 in Chart 4 and Figure 6) [69] but also polyamides (PAMs) (57 and 58 in Chart 4 and Figure 6) [67,68] show extremely high α values from 10 to 20. The PI has spiro-carbons (fluorene) and bulky alkyl side groups and the PAMs have bulky side groups (tris(*tert*-butyl)phenoxy and adamantyl groups). As a result, their d -spacing values (5.9–6.2 Å) [67–69] determined by XRD were larger than those (4.6–5.7 Å) [55] for conventional PIs.

Table 6 summarizes data of α (P_{O_2}/P_{N_2}), α_S (S_{O_2}/S_{N_2}), and α_D (D_{O_2}/D_{N_2}) values from the literature for some of the polymers plotted in Figure 6. For these condensation

polymers (57–59 in Chart 4 and Table 6), the extremely high α values depend not only on α_D but also on α_S . This is much different from Trip-PIMs whose $\alpha (P_{O_2}/P_{N_2})$ values depend only on α_D values because the α_S values are almost unity. Therefore, these extremely high α values could be realized by high α_S values in addition to high α_D values. It suggests the mechanism of this permeation partially involves the SD mechanism.

Figure 9 shows the present situation for PIs. In the plots for PIs reported until the present, the situation is similar to those in Figure 5 and Table 7 [80] and only a few noticeable improvements were reported during the period (50 and 59). They possess kink points or bulky groups in their backbones.

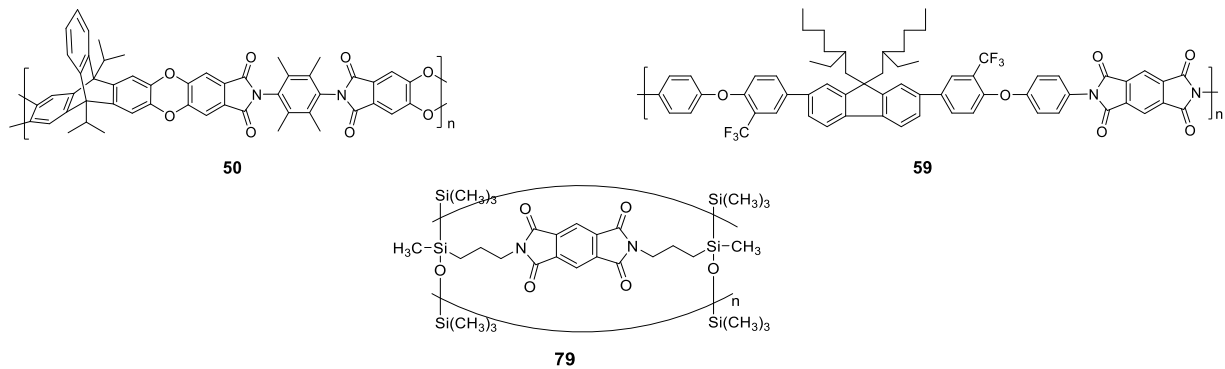


Chart 6. Chemical structures of the membrane polymers in Figure 9 (PIs in 2020).

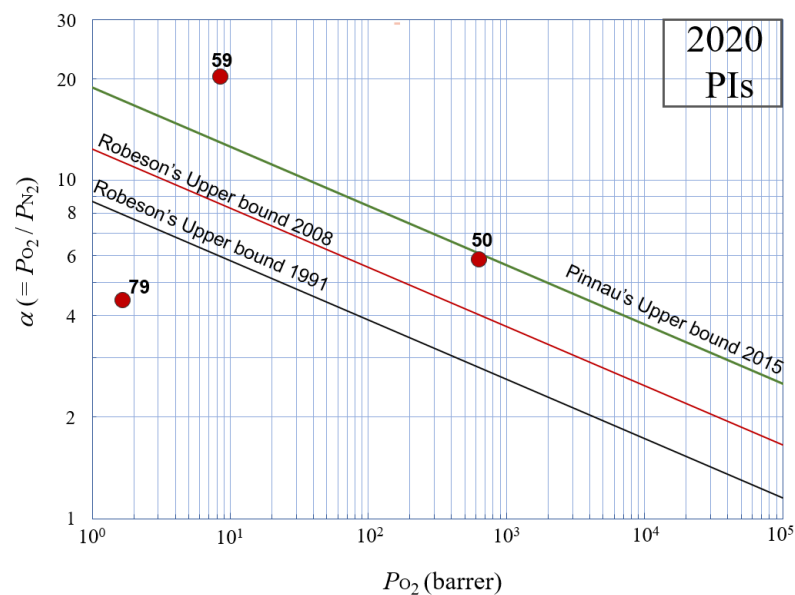


Figure 9. Plots of oxygen permselectivity through polyimides (PI), showing the highest α at each P_{O_2} reported in the literature in 2020. For the data and categorization of the plots, see Table 7, and for the chemical structures of the polymers in the plots, see Chart 6.

Table 7. Categorization and detailed data for the membrane polymers in Figure 9 (PIs in 2020).

Code	P_{O_2} (Barrer)	$\alpha (=P_{O_2}/P_{N_2})$	Thickness (μm)	Feed Gas	Ref. (Year)
50	627	5.86	77	pure	[61] (2014)
59	8.52	20.3	65–75	pure	[69] (2016)
79	1.67	4.44	200	mixed	[80] (2016)

2.3. Tendency of Change in Oxygen Permeation Performances by Changing Chemical Structures of Polymers

As described above as shown in Figures 3–9, it was found that almost all the changes in the oxygen permeation performances by changing the polymer chemical structures are from lower-right positions to upper-left positions and vice versa in these $\alpha - P_{O_2}$ plots. They moved parallel to the upper bound lines in the figures. In other words, whenever their permeability increased, their permselectivity decreased and vice versa. In the case of aging causing physical changes, they also moved parallel to the upper bound lines (for example, Figure 8). However, we found some welcome exceptions in which the permeability and permselectivity increased at the same time as described in this section (Section 2). Here we summarize the exceptions as follows.

I. Changing their backbone structures:

- (1) Linear polymers to ladder polymers (ex. **8**• (PTMSP) to **51**• (a ladder) in Chart 4 and Figures 6 and **8**• (aged PTMSP) to **10**• and **11**• (aged PIMs) in Chart 1 and Figure 3).
- (2) Ladder polymers to ladder polymers with kink points (Trip-PIMs) (ex. **51**• to **47**• in Chart 4 and Figure 6)
- (3) Linear polymers (PIs) to linear polymers with kink points (PIM-PIs) (ex. **22** and **23** to **20** and **21** in Chart 1 and Figure 3)
- (4) Spiro-PIMs to Trip-PIMs (ex. **14**■ (Chart 1) to **47**• (Chart 4) in Figure 8)
- (5) Spiro-PIM (non-aged) (**11**○ in Chart 1 and Figure 8) to locked Spiro-PIM (**44** in Chart 4 and Figure 8)
- (6) c-t PA to c-c PA (ex. **66** in Chart 5 and Figure 7)

Therefore, as can be seen in (1)–(6), it can be concluded that rigidification of main chains is very effective method for producing such simultaneous improvements. In addition to this, introducing contorted sites in the main chains is important.

- (7) Linear polymers to 2D network polymers (**60** and **70** in Chart 5 and Figure 7)

Crosslinking generally forms 3D network structures and often decreases P_{O_2} values, although α values increase effectively (**77** in Figure 7). On the other hand, 2D network structures could enhance both P_{O_2} and α values (**60** and **70** in Chart 5 and Figure 7). Also, soft-crosslinking is suitable for avoidance of loss of P_{O_2} values (**71** and **72** in Chart 5 and Figure 7).

II. Changing their side groups:

- (8) *n*-Propyl Trip-PIM to *iso*-propyl Trip-PIM (**52**• in Chart 4 and Figure 8)
- (9) Spiro-PIM (**11**■ in Chart 1 and Figure 8) to benzospiro-PIM (**10**■ in Chart 1 and Figure 8)
- (10) Introduction of hyperbranched structures (**73**–**75** in Chart 5 and Figure 7)
- (11) PI to PI with bulky pendant groups (**22** and **23** in Chart 1 and Figure 3 to **59** in Chart 4 and Figure 6)
- (12) Methyl Trip-PIM (**53**• in Chart 4 and Figure 8) to unsubstituted Trip-PIM (**47**• in Chart 4 and Figure 8)

Therefore, as can be seen in (8)–(11), it can be concluded that bulkier side groups may create spaces suitable for simultaneously enhancing both P_{O_2} and α values. But sometimes small and flexible substituents can unfavorably occupy spaces between macromolecules. In such cases, the performances were lowered. In fact, such a case was observed in (12). The influence of side groups in polymers with high FFV on their performances is not simple.

3. Simultaneous Improvements of Selectivity and Permeability of Polymer Membranes

In Section 2, performances for pure membranes from mainly only pure polymers whose chemical structures are clear are plotted in Figures 3–9 except for Figure 7 because the main aim of this review is to discuss the relationships between macromolecular structures and their performances. However, the performances usually changed in upper-left

directions or lower-right directions, that is, the changes were often parallel to the upper bound lines when chemical structures were changed. In other words, when P_{O_2} values increased, their α values decreased and vice versa. Although improvement of both P_{O_2} and α values at the same time is very desirable, observations of such improvements were very rare, especially in pure polymer membranes. Therefore, in order to discuss how both P_{O_2} and α values can be increased simultaneously, in this section we will discuss membranes made from physically-modified polymers whose structures are not clear and also composite membranes made from polymers containing porous additives.

3.1. Polymer Modification by Thermal Polymer Reactions

3.1.1. Thermally Rearranged Polymers (TRs)

Thermal rearrangement is one of the effective methods for improving both P_{O_2} and α values simultaneously [81]. Typically, polyimides (PIs) with hydroxyl pendant groups can be thermally converted to poly(benzoxazole)(PBO) by heating around 400 °C (For example, 55 in Chart 4 and Figure 6) [65]. In general, thermally rearranged polymers (TRs) have much higher P_{O_2} values than the original polymers with similar or slightly higher α values. The TRs have both large (8–11 Å) and small (3–5 Å) pores, although the precursor hydroxyl PIs have only intermediate sized (6–7 Å) pores (these sizes were determined by the PALS method). The smaller pores (ultramicro pores) are important for the high α values and the larger pores (micropores) are important for the high P_{O_2} values [48].

3.1.2. Carbon Molecular Sieve Membranes (CMSM)

Organic polymers are used as precursors of carbon molecular sieve membranes (CMSM). The precursor polymers are polyimides (PIs), polysulfones (PSfs), poly(phenylene oxide)s (PPOs) and so on. Figure 10 shows plots of oxygen permeation behaviors for CMSMs. Table 8 lists the detailed data [82–103]. There are many plots for CMSMs above the 2015 upper bound line for organic polymers. Many CMSMs show the best performance among all the membranes and much better performance than organic polymers, although most of them do not show ultrapermeability. CMSMs are generally prepared by pyrolysis by heating of the precursor polymers to more than about 550 °C. Although fabrication of CMSMs that are thin and large in area is generally more difficult and expensive than that of organic polymers, their performance is much better than those of organic polymers. In particular, CMSMs **f**, **g**, **z**, **A**, and **B** have very high α values of more than 20. Although the original P_{O_2} values of the precursor polymers seem to affect those of the resulting CMSMs, these α values for the CMSMs were not influenced by those of the precursor polymers (Chart 7). Since CMSMs **z**, **A**, **B**, and **C** showing high α values of more than 20 were prepared at higher temperatures (at 800 or 900 °C) than usual CMSMs, the temperature seems to be more important for α values than the chemical structures of the precursor polymers.

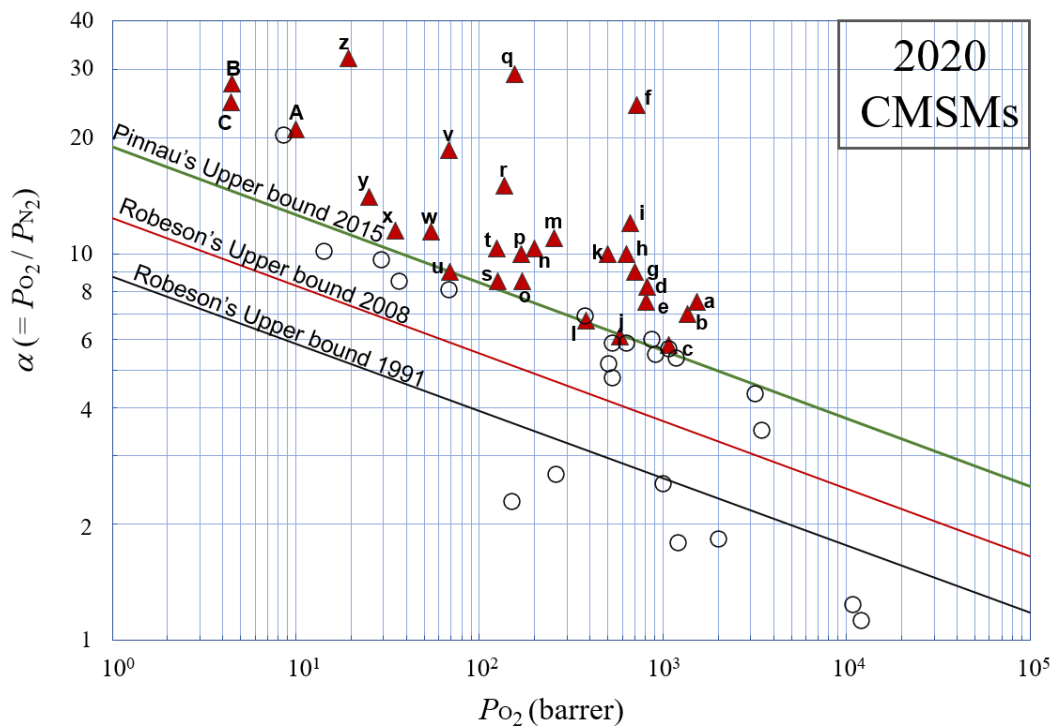


Figure 10. Plots of oxygen permselectivity through carbon molecular sieve membranes (CMSM), showing the highest α at each P_{O_2} reported in the literature in 2020. For the data and categorization of the precursor polymers of the plots, see Table 8, and for the chemical structures of the precursor polymers of the plots, see Chart 7.

Table 8. Categorization and detailed data for CMSMs in Figure 10 (CMSMs in 2020).

Code	Type of Precursors	Pyrolysis Temperature (°C)	P_{O_2} (Barrer)	$\alpha (=P_{O_2}/P_{N_2})$	Thickness (μm)	Ref. (Year)
a	PI	550	1530	7.50	50–80	[82] (2010)
b	PI-PIM	650	1354.5 (4.21)	7.00 (5.90)	45–60	[83] (2019)
c	PI-PIM	600	1071	5.80	80–100	[84] (2013)
d	PI	500	815	8.20	40–50	[85] (1997)
e	PI	550	812 (69.0)	7.50 (4.10)	25–60	[86] (2000)
f	PI	500	723.7 (11.6)	24.2 (3.90)	-	[87] (2008)
g	PI	700	707	9.00	25	[88] (2004)
h	Sulfonated phenolic resin	500	660	12.0	22	[89] (2003)
i	PI	550	630	10.0	40	[90] (2004)
j	PIM(cross-linked)	300	582	6.10	50–60	[91] (2011)
k	PI	700	501	10.0	28	[89] (2004)
l	PI	650	383 (2.46)	6.70 (6.50)	45–60	[83] (2019)
m	PI	700	256	11.0	28	[89] (2004)
n	PI + ZSM	650	200	10.3	50	[92] (2008)
o	PI + Ag	600	170	8.50	20	[93] (2003)
p	PI + MFI zeolite	600	168	10.0	4.5	[94] (2013)
q	PBI	580	156 (0.009)	29.1 (2.02)	-	[95] (2014)
r	PI	700	136	15.0	30	[96] (2005)
s	PI	800	126	8.55	-	[95] (2014)
t	PPO	290	125(25.0)	10.0(4.50)	25–38	[97] (2007)

Table 8. Cont.

Code	Type of Precursors	Pyrolysis Temperature (°C)	P_{O_2} (Barrer)	$\alpha (=P_{O_2}/P_{N_2})$	Thickness (μm)	Ref. (Year)
u	PI	800	69	9.02	-	[95] (2014)
v	PI	800	68	18.5	20–30	[98] (2003)
w	PPO	650	54.7 (7.50)	11.4 (5.50)	25–38	[97] (2007)
x	PI	800	34.8	11.5	113	[99] (1997)
y	PI	800	25.0	14.0	35–60	[100] (2003)
z	PI	800	19.3 (0.27)	32.1 (4.50)	20–30	[98] (2003)
A	PI	900	10.0 (2.00)	21.0 (6.62)	-	[101] (2006)
B	PSF	800	4.50	27.5	-	[102] (2006)
C	PSF	800	4.43 (0.27)	24.6 (3.30)	50	[103] (2009)

[Note] For the codes, see Chart 7.

Since CMSMs are insoluble and amorphous materials which are composed of solely carbon atoms without any organic functional groups, it is difficult to discuss the relationships between macromolecular structures and their performance. Instead, this section focuses on pore sizes in CMSMs.

Figure 11 shows change of performances from the precursor polymers to the resulting CMSMs showing excellent performance. They all change in the direction of upper-right significantly, that is, simultaneous enhancements of P_{O_2} and α values are observed. In particular, the changes of the performance from their precursors to the CMSMs **f**, **g**, **z**, **A**, and **C** are very large. These desirable changes come about because the CMSMs may have both ultramicropores contributing high α and micropores contributing high P_{O_2} , although the precursor polymers may have only intermediate-sized pores [101]. These high α values were caused by their high α_D values. Their α_S values were almost at unity because CMSMs had no functional groups which could selectively interact with gas molecules. CMSM **A** (in Figures 9 and 10) has performance ($P_{O_2} = 10$, $\alpha = 21$) similar to a polyimide ($P_{O_2} = 8.5$, $\alpha = 20$; Figure 6 and Chart 4, 59) with bulky pendant groups showing the highest α value among all the polymers described in Section 2.2.3. However, the α value of CMSM depends only on the α_D value (=17), but the α value of the polyimide depended both on the α_D (=7) and α_S values (=3). (Table 6) Their separation mechanisms are different. Generally, both ultramicropores and micropores were created simultaneously by pyrolysis of precursor polymers such as polyimides. When the pyrolysis temperature was high, the size of the ultramicropores became smaller. Therefore, CMSMs prepared at higher temperatures showed higher α values and lower P_{O_2} values. In other words, by increasing the pyrolysis temperature, α values increase and P_{O_2} values decrease [101].

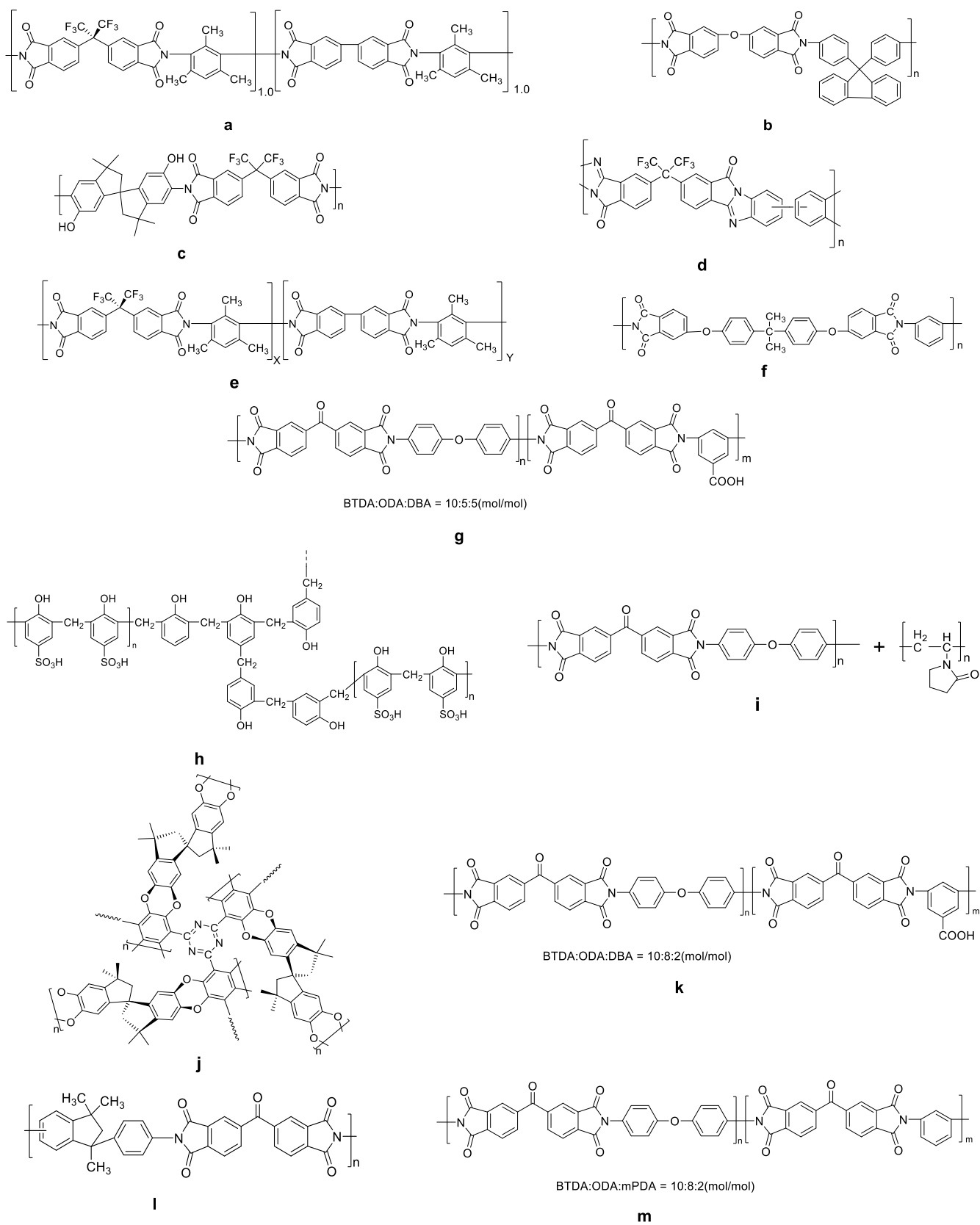


Chart 7. Cont.

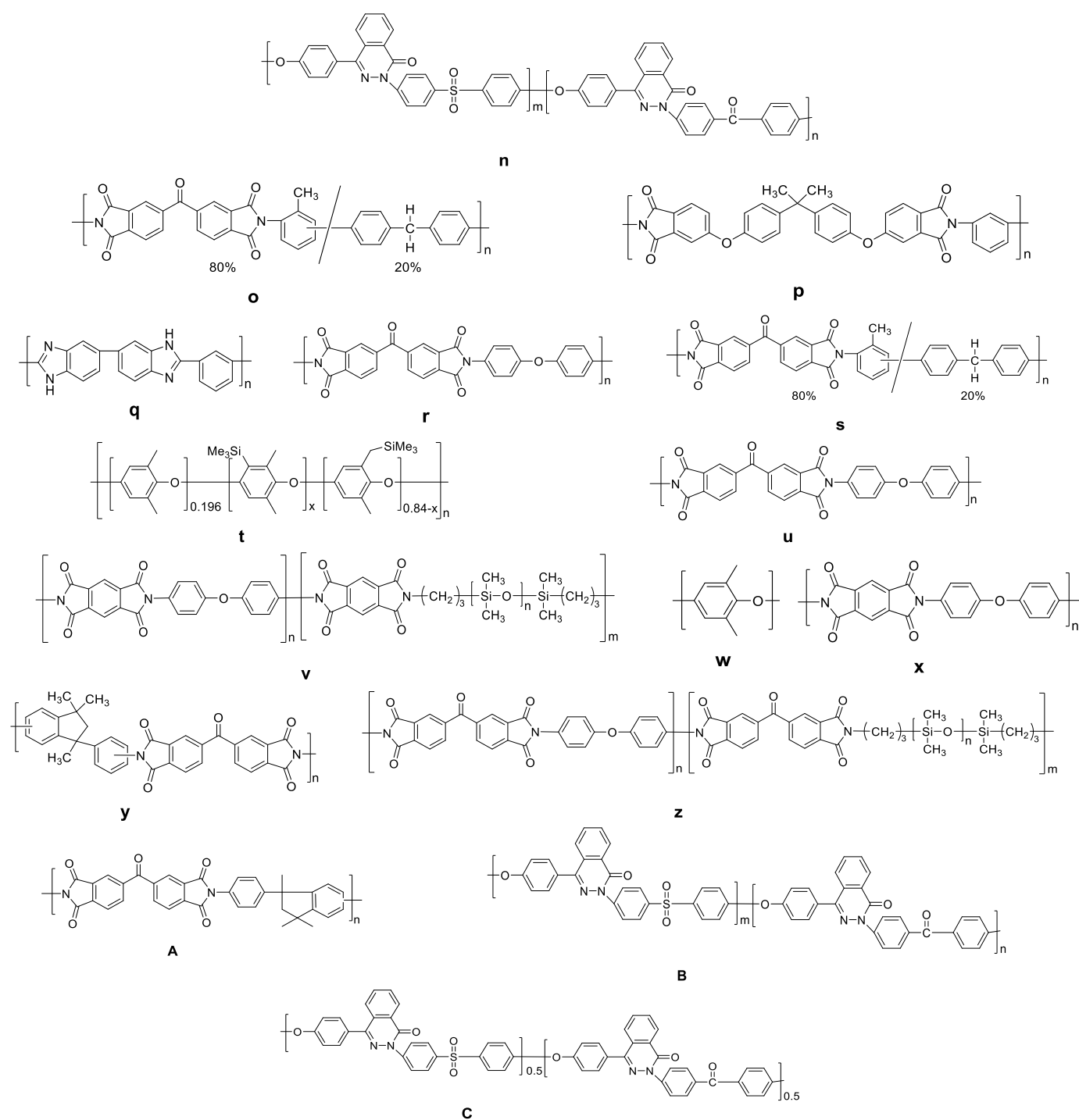


Chart 7. Chemical structures of the precursor polymers of CMSMs in Figure 10 (CMSMs in 2020).

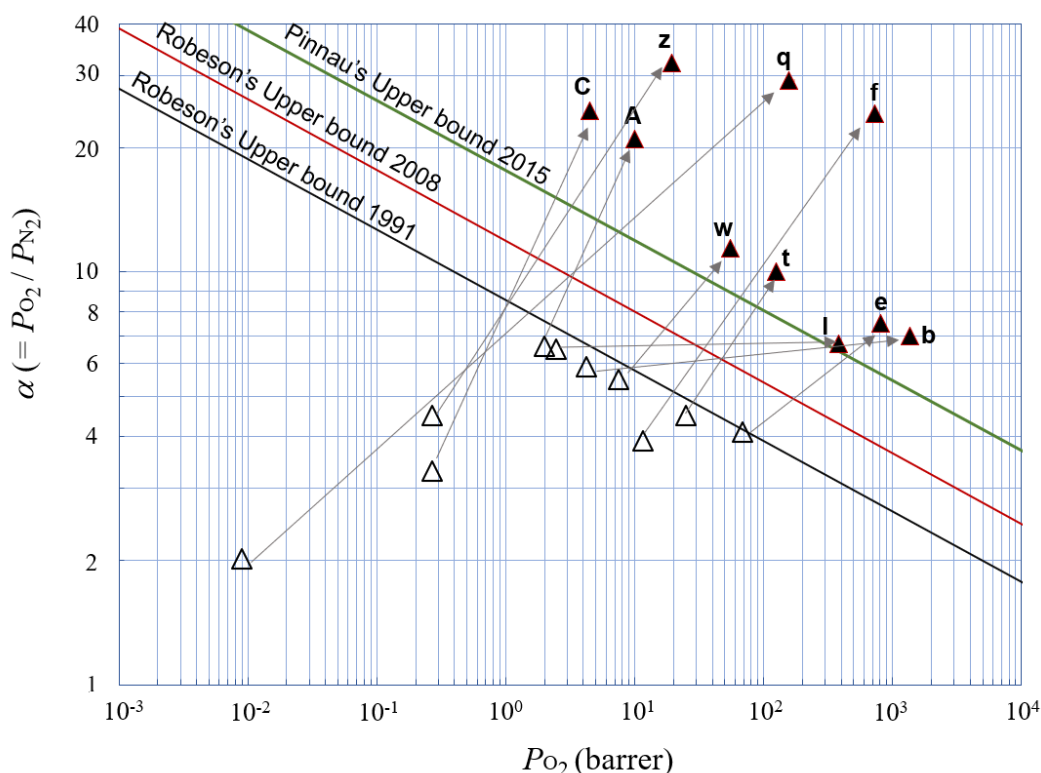


Figure 11. Change in the α and P_{O_2} from the precursor polymers to carbon molecular sieve membranes (CMSMs). For the codes, data and categorization of the precursor polymers of the plots, see Chart 7.

3.2. Polymer Membrane Modification by Blending with Microporous Additives—Mixed Matrix Membranes (MMMs)

As described in Section 3.1, in order to enhance P_{O_2} and α values simultaneously for a membrane, both ultramicropores and micropores should be created in the membrane. Preparation of CMSMs by pyrolysis of polymers is a very suitable method. However, control of the membrane preparation process and the pore sizes are still challenging. As another methodology for preparation of membranes with good mechanical strength and micropores whose sizes are well-controlled, mixed matrix membranes (MMMs) have been recently developed [104–107]. Typically, an MMM consists of a soluble amorphous organic polymer which shows good membrane-forming ability as a matrix and insoluble crystalline inorganic porous compounds as an additive or a filler which has no membrane-forming ability and well-defined micro- or ultramicropores. In this section, we will describe examples of the simultaneous increase in P_{O_2} and α values found in the studies on MMMs. Because such examples are very rare, especially for separation of the mixture of O_2 and N_2 whose size is 3.46 Å and 3.64 Å, respectively (their size difference is 0.18 Å), here we will include results from studies on separation performances for the other mixtures. For example, the mixture of CO_2 and CH_4 whose size is 3.30 Å and 3.80 Å, respectively (their size difference is 0.50 Å) and the mixture of CO_2 and N_2 whose size is 3.30 Å and 3.64 Å, respectively (their size difference is 0.34 Å), are described.

3.2.1. Required Conditions for Simultaneous Improvements of Selectivity and Permeability by the MMM Method

In order to use effectively both the roles of matrix polymers and porous additives in MMMs, it is necessary that the two components do not interact negatively with each other and their boundaries produce no defects. To avoid forming such defects, compatibility of polymers with additives in MMMs is important.

3.2.2. Types of Microporous Additives

(1) Zeolites [104]

In combinations of zeolite 4A (pore size: 3.8 Å) (25 wt%) [108] and polysulfones, and zeolite 5A (pore size: 4.8 Å) (50 wt%) and poly(ether sulfone) [109], simultaneous improvements were reported from $P_{O_2} = 1.3$ barrer and $\alpha = 5.9$ to $P_{O_2} = 1.8$ barrer and $\alpha = 7.7$, and from $P_{O_2} = 0.47$ barrer and $\alpha = 5.8$ to $P_{O_2} = 0.70$ barrer and $\alpha = 7.4$, respectively. On the other hand, in the combinations of zeolite 4A and poly(vinyl acetate), poly(ether imide), or polyimide, α increased but P_{O_2} decreased. The decrease may be caused by blocking of their micropores in the zeolite by the polymers. The selection of the matrix polymers is important.

(2) Metal organic frameworks (MOF) [105]

Because metal organic frameworks (MOF) include organic ligands, the compatibility of MOFs with organic polymers should be higher than that of purely inorganic zeolites. In addition, to reduce the formation of defects between polymers and MOF fillers, introduction of functional groups such as amino or acid groups was effective. For example, MMMs of sulfonated MOFs with sulfonated polyimides showed higher P_{CO_2} and P_{CO_2}/P_{CH_4} than those of non-modified polyimides [110]. MMMs of an amine-functionalized MOF and a polyimide also showed higher P_{CO_2} and P_{CO_2}/P_{CH_4} than the polyimide itself [111,112]. Similarly, in the combination of a polyimide-grafted MOF and a polyimide, a simultaneous increase of P_{CO_2} and P_{CO_2}/P_{CH_4} values was observed [113].

(3) Microporous organic cages (POC) [107]

Because microporous organic cages (POC) are purely organic compounds, the compatibility of POCs with organic polymers should be much higher than that of MOFs described above. For example, in an MMM consisting of an imine POC and PIM-1, by addition of the POC, P_{CO_2} and P_{CO_2}/P_{N_2} simultaneously increased [114]. In the case of the mixture of O_2 and N_2 , the addition of a β -cyclodextrin (the pore size is 6.0–6.4 Å) as a POC to a polyimide resulted in only a slight increase in α with a slight decrease in P_{O_2} [115].

3.2.3. Sizes (Nanocrystals), Shapes (Nanosheets), and Assembled Structures of Microporous Additives

The sizes of additives in MMMs showed large effects on performance. For example, when nanocrystals of a MOF were added to a polyimide, both the PC_2H_2 and PC_2H_2/PC_2H_4 values were enhanced, although when the bulk MOF was used the PC_2H_2 increased but PC_2H_2/PC_2H_4 decreased [116]. The nanosize crystals may avoid the production of defects. The shape of additives also had great effects. In the case of a nanosheet of a MOF accumulated on a macroporous support, by suppressing stackings of the nanosheets, P_{H_2} and P_{H_2}/P_{CO_2} increased simultaneously [117]. An MMM based on polybenzimidazole using a nanosheet of a MOF showed simultaneous increases in P_{H_2} and P_{H_2}/P_{CO_2} . On the other hand, when nanocrystals were used instead, P_{H_2}/P_{CO_2} increased but P_{H_2} decreased [118]. Similarly, only a nanosheet of a MOF was effective for enhancing P_{CO_2}/P_{CH_4} (although P_{CO_2} decreased), while nanocrystals of the MOF were not effective [119].

4. Concluding Remarks

4.1. High Permeable Linear Polymers, PTMSP and PIMs

The ultrahigh P_{O_2} ($>10^4$) of very rigid polymers consisting of alternating double bonds with bulky substituents, that is, PTMSP (8 in Chart 1 and Figure 3), was reported by Prof. Masuda in 1983 [45] and it was confirmed that it contains micropores and its permeation is based on the MS mechanism. Then a new ladder polymer with spirocarbons as contorted points, that is, PIM-1 (11 in Chart 1 and Figure 3), was developed by Prof. Budd and McKeown in 2005 [29]. With the advent of this new polymer, the original Robeson's 1991 upper bound [10] was revised in 2008 [12]. Finally, Prof. Pinnau updated Robeson's 2008 upper bound in 2015 after several Trip-PIMs emerged (47, 50, and 52 in Chart 4 and

Figure 6) in 2014 [59,61,63]. Recently, the best PIM having higher ultrapermeability and a very high α was reported by Prof. McKeown in 2017 [44]. Furthermore, it was reported that a new polyimide (polymer 25 in Figure 6) having bulky substituents showed extremely high α (=20.3) by Prof. Banerjee in 2016 [69]. The rate of progress during 2014–2020 was much faster than that during 1991–2013, although the former term (7 years) is much shorter than the latter (23 years).

The separations of these high-performance polymers are based on mainly α_D , particularly for polymers with high P_{O_2} values such as PTMSP and PIMs. (Although excellent research on oxygen permselective membranes based on α_S using metal complexes as oxygen carriers has been carried out by Prof. Nishide, this review does not describe this work because it is outside its scope [120]) In other words, it depends on the MS mechanism. Therefore, the size distribution of their micro- and ultramicropores is decisive and the control of their sizes is important. However, since the micropores are created as spaces between macromolecules, the control of the size is not easy and in addition their stability is low. In fact, their P_{O_2} values decreased significantly with time (see Figure 8). This is a big problem for these polymers in terms of practical applications.

4.2. High Permselective Inorganic Membranes, CMSM and Graphene

When the chemical structure of a polymer was changed, their performances often changed in the direction of the upper-left or lower-right in the $\alpha - P_{O_2}$ graphs. In other words, their direction of change is parallel to the upper bound lines. The most desirable change of improvements of their performances is a movement in the direction of the upper-right, i.e., a simultaneous increase in P_{O_2} and α . However, such examples were very rare, as described above. Treatment with physical factors such as heat [121] and light [122] resulted in an increase in α with a decrease in P_{O_2} and vice versa. However, we noticed extreme changes in the direction of the upper-right for the preparation of CMSMs from their precursor polymers by heating at 550–800 °C (Figure 11). Although heat treatment of polymer membranes usually affects just high-ordered structures, in this case of formation of CMSMs, changes in chemical structures happened, that is, carbonization with evolution of organic vapors and gases. However, the resulting CMSMs were insoluble and amorphous and, therefore, it is not easy to prepare wide thin membranes of CMSMs like polymer membranes. In addition, it is difficult to know their precise chemical structures from NMR and XRD. The details of the chemical structures are not known but it was thought they may contain graphene sheets. Although graphene macromolecules themselves have no internal pores and, therefore, no filtration functions based on the MS mechanism, the 2D shape seems to be suitable for enhancing performances. (Although some graphenes were applied to gas separation membranes [123,124], their selective permeation occurred during permeation through spaces between graphene sheets or internal defects in graphene sheets.)

4.3. Promising Membranes from Regularly Networked Organic Polymers, 2DPs

Some researchers reported networked 2DPs or nanosheets which are similar to graphene but have micropores whose sizes are similar to those of gas molecules and tried to apply them for gas separation membranes. An example of synthetic 2DPs is a two-dimensional covalent framework (2DCOF) [125]. However, since COFs are crystalline and insoluble, reports of successful applications to oxygen separation membranes were almost zero. Instead we tried to use some kinds of networked polymers and the related polymers made from linear polymers described in Section 2.2.1(2). By adding networked structures, α values often increased but P_{O_2} decreased. In the case of networks prepared by short flexible crosslinking, the decrease of P_{O_2} was suppressed [76]. In particular, when networked 2DPs was introduced in situ into linear polymers in the membrane state, both α and P_{O_2} increased [75]. Although application of 2D materials to separation membranes was reported recently, there have been very few studies on gas separation. In particular, to the best of our knowledge, there have been no reports on the application of 2DP to oxygen permselective membranes [126]. Judging from all these reports, membranes from

organic polymers containing organic network 2DPs inside the membranes seem to be a very promising avenue to pursue.

Supplementary Materials: The following are available online at <https://www.mdpi.com/article/10.3390/polym13173012/s1>, S1: Contents of this review.

Author Contributions: Writing—original draft preparation, T.A. and J.W.; writing—review and editing, T.A., J.W.; investigation, Z.S., Y.Z., H.J.; discussion, M.T., T.K. All authors have read and agreed to the published version of the manuscript.

Funding: This research was funded by the Scientific Research Project of basic Scientific Research Business expenses of Provincial Colleges and Universities in Heilongjiang Province [135309346]; Technology Foundation for Selected Overseas Chinese, Ministry of Human Resources and Social Security of Heilongjiang Province ([2016] 75 (No.430237)).

Conflicts of Interest: The authors declare no conflict of interest.

References

1. Aoki, T. Macromolecular design of permselective membranes. *Prog. Polym. Sci.* **1999**, *24*, 951–993. [[CrossRef](#)]
2. McKeown, N.B.; Budd, P.M.; Msayib, K.J.; Ghanem, B.S.; Kingston, H.J.; Tattershall, C.E.; Makhseed, S.; Reynolds, K.J.; Fritsch, D. Polymers of Intrinsic Microporosity (PIMs): Bridging the Void between Microporous and Polymeric Materials. *Chem. Eur. J.* **2005**, *11*, 2610–2620. [[CrossRef](#)]
3. Budd, P.M.; McKeown, N. Highly permeable polymers for gas separation membranes. *Polym. Chem.* **2010**, *1*, 63–68. [[CrossRef](#)]
4. Usman, M.; Ahmed, A.; Yu, B.; Peng, Q.; Shen, Y.; Cong, H. A review of different synthetic approaches of amorphous intrinsic microporous polymers and their potential applications in membrane-based gases separation. *Eur. Polym. J.* **2019**, *120*, 109262. [[CrossRef](#)]
5. Zhou, H.; Jin, W. Membranes with Intrinsic Micro-Porosity: Structure, Solubility, and Applications. *Membranes* **2019**, *9*, 3. [[CrossRef](#)]
6. Baker, R.W.; Low, B.T. Gas Separation Membrane Materials: A Perspective. *Macromolecules* **2014**, *47*, 6999–7013. [[CrossRef](#)]
7. Koros, W.J.; Zhang, C. Materials for next-generation molecularly selective synthetic membranes. *Nat. Mater.* **2017**, *16*, 289–297. [[CrossRef](#)]
8. Sanders, D.F.; Smith, Z.P.; Guo, R.; Robeson, L.M.; McGrath, J.E.; Paul, D.R.; Freeman, B.D. Energy-efficient polymeric gas separation membranes for a sustainable future: A review. *Polymer* **2013**, *54*, 4729–4761. [[CrossRef](#)]
9. Wijmans, J.G.; Baker, R.W. The solution-diffusion model: A review. *J. Membr. Sci.* **1995**, *107*, 1–21. [[CrossRef](#)]
10. Robeson, L.M. Correlation of separation factor versus permeability for polymeric membranes. *J. Membr. Sci.* **1991**, *62*, 165–185. [[CrossRef](#)]
11. Freeman, B.D. Basis of Permeability/Selectivity Trade-off Relations in Polymeric Gas Separation Membranes. *Macromolecules* **1999**, *32*, 375–380. [[CrossRef](#)]
12. Robeson, L.M. The upper bound revisited. *J. Membr. Sci.* **2008**, *320*, 390–400. [[CrossRef](#)]
13. Swaidan, R.; Ghanem, B.; Pinnau, I. Fine-Tuned Intrinsically Ultramicroporous Polymers Redefine the Permeability/Selectivity Upper Bounds of Membrane-Based Air and Hydrogen Separations. *ACS Macro Lett.* **2015**, *4*, 947–951. [[CrossRef](#)]
14. Hu, Y.; Shiotsuki, M.; Sanda, F.; Freeman, B.; Masuda, T. Synthesis and Properties of Indan-Based Polyacetylenes That Feature the Highest Gas Permeability among All the Existing Polymers. *Macromolecules* **2008**, *41*, 8525–8532. [[CrossRef](#)]
15. Hu, Y.; Shiotsuki, M.; Sanda, F.; Masuda, T. Synthesis and extremely high gas permeability of polyacetylenes containing polymethylated indan/tetrahydronaphthalene moieties. *Chem. Commun.* **2007**, 4269–4270. [[CrossRef](#)]
16. Morisato, A.; Pinnau, I. Synthesis and gas permeation properties of poly(4-methyl-2-pentyne). *J. Membr. Sci.* **1996**, *121*, 243–250. [[CrossRef](#)]
17. Fukui, A.; Hattori, K.; Hu, Y.; Shiotsuki, M.; Sanda, F.; Masuda, T. Synthesis, characterization, and high gas permeability of poly(diarylacetylene)s having fluorenyl groups. *Polymer* **2009**, *50*, 4159–4165. [[CrossRef](#)]
18. Sakaguchi, T.; Yumoto, K.; Shida, Y.; Shiotsuki, M.; Sanda, F.; Masuda, T. Synthesis, properties, and gas permeability of novel poly(diarylacetylene) derivatives. *J. Polym. Sci. Part A Polym. Chem.* **2006**, *44*, 5028–5038. [[CrossRef](#)]
19. Kouzai, H.; Masuda, T.; Higashimura, T. Synthesis and properties of poly (diphenylacetylenes) having aliphatic para-substituents. *J. Polym. Sci. Part A Polym. Chem.* **1994**, *32*, 2523–2530. [[CrossRef](#)]
20. Kwak, G.; Aoki, T.; Kaneko, T. Synthesis and stable high oxygen permeability of poly(diphenylacetylene)s with two or three trimethylsilyl groups. *Polymer* **2002**, *43*, 1705–1709. [[CrossRef](#)]
21. Yampol'Skii, Y.P.; Shishatskii, S.M.; Shantorovich, V.P.; Antipov, E.M.; Kuzmin, N.N.; Rykov, S.V.; Khodjaeva, V.L.; Platé, N.A. Transport characteristics and other physicochemical properties of aged poly(1-(trimethylsilyl)-1-propyne). *J. Appl. Polym. Sci.* **1993**, *48*, 1935–1944. [[CrossRef](#)]
22. Tsuchihara, K.; Masuda, T.; Higashimura, T. Polymerization of silicon-containing diphenylacetylenes and high gas permeability of the product polymers. *Macromolecules* **1992**, *25*, 5816–5820. [[CrossRef](#)]

23. Bezzu, C.G.; Carta, M.; Ferrari, M.-C.; Jansen, J.C.; Monteleone, M.; Esposito, E.; Fuoco, A.; Hart, K.; Liyana-Arachchi, T.P.; Colina, C.M.; et al. The synthesis, chain-packing simulation and long-term gas permeability of highly selective spirobifluorene-based polymers of intrinsic microporosity. *J. Mater. Chem. A* **2018**, *6*, 10507–10514. [[CrossRef](#)]
24. Bezzu, C.G.; Carta, M.; Tonkins, A.; Jansen, J.; Bernardo, P.; Bazzarelli, F.; McKeown, N.B. A Spirobifluorene-Based Polymer of Intrinsic Microporosity with Improved Performance for Gas Separation. *Adv. Mater.* **2012**, *24*, 5930–5933. [[CrossRef](#)]
25. Swaidan, R.; Ghanem, B.; Litwiller, E.; Pinnau, I. Physical Aging, Plasticization and Their Effects on Gas Permeation in “Rigid” Polymers of Intrinsic Microporosity. *Macromolecules* **2015**, *48*, 6553–6561. [[CrossRef](#)]
26. Ghanem, B.S.; McKeown, N.B.; Budd, P.M.; Selbie, J.D.; Fritsch, D. High-Performance Membranes from Polyimides with Intrinsic Microporosity. *Adv. Mater.* **2008**, *20*, 2766–2771. [[CrossRef](#)]
27. Ma, X.; Salinas, O.; Litwiller, E.; Pinnau, I. Novel Spirobifluorene- and Dibromospirobifluorene-Based Polyimides of Intrinsic Microporosity for Gas Separation Applications. *Macromolecules* **2013**, *46*, 9618–9624. [[CrossRef](#)]
28. Du, N.; Robertson, G.P.; Song, J.; Pinnau, I.; Guiver, M.D. High-Performance Carboxylated Polymers of Intrinsic Microporosity (PIMs) with Tunable Gas Transport Properties. *Macromolecules* **2009**, *42*, 6038–6043. [[CrossRef](#)]
29. Budd, P.M.; Msayib, K.J.; Tattershall, C.E.; Ghanem, B.S.; Reynolds, K.J.; McKeown, N.; Fritsch, D. Gas separation membranes from polymers of intrinsic microporosity. *J. Membr. Sci.* **2005**, *251*, 263–269. [[CrossRef](#)]
30. Du, N.; Robertson, G.P.; Song, J.; Pinnau, I.; Thomas, S.; Guiver, M. Polymers of Intrinsic Microporosity Containing Trifluoromethyl and Phenylsulfone Groups as Materials for Membrane Gas Separation. *Macromolecules* **2008**, *41*, 9656–9662. [[CrossRef](#)]
31. Lin, W.-H.; Chung, T.-S. Gas permeability, diffusivity, solubility, and aging characteristics of 6FDA-durene polyimide membranes. *J. Membr. Sci.* **2001**, *186*, 183–193. [[CrossRef](#)]
32. Qiu, W.; Xu, L.; Chen, C.-C.; Paul, D.R.; Koros, W.J. Gas separation performance of 6FDA-based polyimides with different chemical structures. *Polymer* **2013**, *54*, 6226–6235. [[CrossRef](#)]
33. Sen, S.K.; Banerjee, S. Spiro-biindane containing fluorinated poly(ether imide)s: Synthesis, characterization and gas separation properties. *J. Membr. Sci.* **2010**, *365*, 329–340. [[CrossRef](#)]
34. Kim, Y.-H.; Kim, H.-S.; Kwon, S.-K. Synthesis and Characterization of Highly Soluble and Oxygen Permeable New Polyimides Based on Twisted Biphenyl Dianhydride and Spirobifluorene Diamine. *Macromolecules* **2005**, *38*, 7950–7956. [[CrossRef](#)]
35. Al-Masri, M.; Kricheldorf, A.H.R.; Fritsch, D. New Polyimides for Gas Separation. 1. Polyimides Derived from Substituted Terphenylenes and 4,4'-(Hexafluoroisopropylidene)diphthalic Anhydride. *Macromolecules* **1999**, *32*, 7853–7858. [[CrossRef](#)]
36. Aoki, T.; Nakahara, H.; Hayakawa, Y.; Kokai, M.; Oikawa, E. Trimethylsilyl-group containing polyphenylacetylenes for oxygen and ethanol permselective membranes. *J. Polym. Sci. Part A Polym. Chem.* **1994**, *32*, 849–858. [[CrossRef](#)]
37. Hayakawa, Y.; Nishida, M.; Aoki, T.; Muramatsu, H. Synthesis of poly(phenylacetylene)s containing trifluoromethyl groups for gas permeable membrane. *J. Polym. Sci. Part A Polym. Chem.* **1992**, *30*, 873–877. [[CrossRef](#)]
38. Masuda, T.; Iguchi, Y.; Tang, B.-Z.; Higashimura, T. Diffusion and solution of gases in substituted polyacetylene membranes. *Polymer* **1988**, *29*, 2041–2049. [[CrossRef](#)]
39. Masuda, T.; Matsumoto, T.; Yoshimura, T.; Higashimura, T. Synthesis and Properties of Poly[1-(*n*-alkylthio)-1-propynes]. *Macromolecules* **1990**, *23*, 4902–4907. [[CrossRef](#)]
40. Seki, H.; Masuda, T.; Higashimura, T. Synthesis and Properties of Poly(phenylacetylenes) Having *o*-Silylmethyl Groups. *J. Polym. Sci. Part A Polym. Chem.* **1995**, *33*, 117–124. [[CrossRef](#)]
41. Fujita, Y.; Misumi, Y.; Tabata, M.; Masuda, T. Synthesis, Geometric Structure, and Properties of Poly(phenylacetylenes) with Bulky Para-Substituents. *J. Polym. Sci. Part A Polym. Chem.* **1998**, *36*, 3157–3163. [[CrossRef](#)]
42. Aoki, T.; Shinohara, K.-I.; Kaneko, T.; Oikawa, E. Enantioselective Permeation of Various Racemates through an Optically Active Poly[1-[dimethyl(10-pinanyl)silyl]-1-propyne] Membrane. *Macromolecules* **1996**, *29*, 4192–4198. [[CrossRef](#)]
43. Teraguchi, M.; Masuda, T. Synthesis and Properties of Polyacetylenes with Adamantyl Groups. *J. Polym. Sci. Part A Polym. Chem.* **1999**, *37*, 4546–4553. [[CrossRef](#)]
44. Rose, I.; Bezzu, C.G.; Carta, M.; Comesaña-Gándara, B.; Lasseguette, E.; Ferrari, M.-C.; Bernardo, P.; Clarizia, G.; Fuoco, A.; Jansen, J.C.; et al. Polymer ultrapermeability from the inefficient packing of 2D chains. *Nat. Mater.* **2017**, *16*, 932–937. [[CrossRef](#)]
45. Masuda, T.; Isobe, E.; Higashimura, T.; Takada, K. Poly[1-(trimethylsilyl)-1-propyne]: A New High Polymer Synthesized with Transition-Metal Catalysts and Characterized by Extremely High Gas Permeability. *J. Am. Chem. Soc.* **1983**, *105*, 7473–7474. [[CrossRef](#)]
46. Nagai, K.; Masuda, T.; Nakagawa, T.; Freeman, B.; Pinnau, I. Poly[1-(trimethylsilyl)-1-propyne] and related polymers: Synthesis, properties and functions. *Prog. Polym. Sci.* **2001**, *26*, 721–798. [[CrossRef](#)]
47. Wang, X.-Y.; Lee, K.M.; Lu, Y.; Stone, M.T.; Sanchez, I.; Freeman, B. Cavity size distributions in high free volume glassy polymers by molecular simulation. *Polymer* **2004**, *45*, 3907–3912. [[CrossRef](#)]
48. Han, S.H.; Misdan, N.; Kim, S.; Doherty, C.; Hill, A.J.; Lee, Y.M. Thermally Rearranged (TR) Polybenzoxazole: Effects of Diverse Imidization Routes on Physical Properties and Gas Transport Behaviors. *Macromolecules* **2010**, *43*, 7657–7667. [[CrossRef](#)]
49. Ghanem, B.S.; Swaidan, R.; Litwiller, E.; Pinnau, I. Ultra-Microporous Triptycene-based Polyimide Membranes for High-Performance Gas Separation. *Adv. Mater.* **2014**, *26*, 3688–3692. [[CrossRef](#)]
50. Shantarovich, V.P.; Azamatova, Z.K.; Yampolskii, Y.P. Free-Volume Distribution of High Permeability Membrane Materials Probed by Positron Annihilation. *Macromolecules* **1998**, *31*, 3963–3966. [[CrossRef](#)]

51. Aoki, T.; Oikawa, E.; Hayakawa, Y.; Nishida, M. Improvement of oxygen permselectivity through polydimethylsiloxane and poly(1-trimethylsilylpropyne) films by the addition of a small amount of poly(trifluoromethyl substituted arylacetylene). *J. Membr. Sci.* **1991**, *57*, 207–216. [[CrossRef](#)]
52. Lin, W.-H.; Vora, R.H.; Chung, T.-S. Gas Transport Properties of 6FDA-durene/1,4-phenylenediamine (pPDA) Copolyimides. *J. Polym. Sci. Part B Polym. Phys.* **2000**, *38*, 2703–2713. [[CrossRef](#)]
53. Liu, Y.; Pan, C.; Ding, M.; Xu, J. Gas permeability and permselectivity of polyimides prepared from phenylenediamines with methyl substitution at the ortho position. *Polym. Int.* **1999**, *48*, 832–836. [[CrossRef](#)]
54. Tanaka, K.; Okano, M.; Toshino, H.; Kita, H.; Okamoto, K.-I. Effect of methyl substituents on permeability and permselectivity of gases in polyimides prepared from methyl-substituted phenylenediamines. *J. Polym. Sci. Part B Polym. Phys.* **1992**, *30*, 907–914. [[CrossRef](#)]
55. Koros, W.; Fleming, G.; Jordan, S.; Kim, T.; Hoehn, H. Polymeric Membrane Materials for Solution-Diffusion Based Permeation Separations. *Prog. Polym. Sci.* **1988**, *13*, 339–401. [[CrossRef](#)]
56. Kim, T.; Koros, W.; Husk, G.; O'Brien, K. Relationship between Gas Separation Properties and Chemical Structure in a Series of Aromatic Polyimides. *J. Membr. Sci.* **1988**, *37*, 45–62. [[CrossRef](#)]
57. Zhang, J.; Kang, H.; Martin, J.W.; Zhang, S.; Thomas, S.; Merkel, T.C.; Jin, J. The Enhancement of Chain Rigidity and Gas Transport Performance of Polymers of Intrinsic Microporosity via Intramolecular Locking of the Spiro-Carbon. *Chem. Commun.* **2016**, *52*, 6553–6556. [[CrossRef](#)]
58. Rose, I.; Carta, M.; Malpass-Evans, R.; Ferrari, M.-C.; Bernardo, P.; Clarizia, G.; Jansen, J.; McKeown, N.B. Highly Permeable Benzotriptycene-Based Polymer of Intrinsic Microporosity. *ACS Macro Lett.* **2015**, *4*, 912–915. [[CrossRef](#)]
59. Carta, M.; Croad, M.; Malpass-Evans, R.; Jansen, J.C.; Bernardo, P.; Clarizia, G.; Friess, K.; Lanč, M.; McKeown, N.B. Triptycene Induced Enhancement of Membrane Gas Selectivity for Microporous Tröger's Base Polymers. *Adv. Mater.* **2014**, *26*, 3526–3531. [[CrossRef](#)]
60. Zhu, Z.; Zhu, J.; Li, J.; Ma, X. Enhanced Gas Separation Properties of Tröger's Base Polymer Membranes Derived from Pure Triptycene Diamine Regioisomers. *Macromolecules* **2020**, *53*, 1573–1584. [[CrossRef](#)]
61. Swaidan, R.; Al-Saeedi, M.; Ghanem, B.; Litwiller, E.; Pinnau, I. Rational Design of Intrinsically Ultramicroporous Polyimides Containing Bridgehead-Substituted Triptycene for Highly Selective and Permeable Gas Separation Membranes. *Macromolecules* **2014**, *47*, 5104–5114. [[CrossRef](#)]
62. Ma, X.; Lai, H.W.H.; Wang, Y.; Alhazmi, A.; Xia, Y.; Pinnau, I. Facile Synthesis and Study of Microporous Catalytic Arene-Norbornene Annulation-Tröger's Base Ladder Polymers for Membrane Air Separation. *ACS Macro Lett.* **2020**, *9*, 680–685. [[CrossRef](#)]
63. Ghanem, B.S.; Swaidan, R.; Ma, X.; Litwiller, E.; Pinnau, I. Energy-Efficient Hydrogen Separation by AB-Type Ladder-Polymer Molecular Sieves. *Adv. Mater.* **2014**, *26*, 6696–6700. [[CrossRef](#)]
64. Malpass-Evans, R.; Rose, I.; Fuoco, A.; Bernardo, P.; Clarizia, G.; McKeown, N.B.; Jansen, J.C.; Carta, M. Effect of Bridgehead Methyl Substituents on the Gas Permeability of Tröger's-Base Derived Polymers of Intrinsic Microporosity. *Membranes* **2020**, *10*, 62. [[CrossRef](#)] [[PubMed](#)]
65. Luo, S.; Zhang, Q.; Zhu, L.; Lin, H.; Kazanowska, B.A.; Doherty, C.M.; Hill, A.J.; Gao, P.; Guo, R. Highly Selective and Permeable Microporous Polymer Membranes for Hydrogen Purification and CO₂ Removal from Natural Gas. *Chem. Mater.* **2018**, *30*, 5322–5332. [[CrossRef](#)]
66. Olvera, L.I.; Rodríguez-Molina, M.; Ruiz-Treviño, F.A.; Zolotukhin, M.G.; Fomine, S.; Cárdenas, J.; Gaviño, R.; Alexandrova, L.; Toscano, R.A.; Martínez-Mercado, E. A Highly Soluble, Fully Aromatic Fluorinated 3D Nanostructured Ladder Polymer. *Macromolecules* **2017**, *50*, 8480–8486. [[CrossRef](#)]
67. Bera, D.; Padmanabhan, V.; Banerjee, S. Highly Gas Permeable Polyamides Based on Substituted Triphenylamine. *Macromolecules* **2015**, *48*, 4541–4554. [[CrossRef](#)]
68. Bera, D.; Bandyopadhyay, P.; Ghosh, S.; Banerjee, S.; Padmanabhan, V. Highly gas permeable aromatic polyamides containing adamantane substituted triphenylamine. *J. Membr. Sci.* **2015**, *474*, 20–31. [[CrossRef](#)]
69. Ghosh, S.; Banerjee, S. 9-Alkylated Fluorene-Based Poly(Ether Imide)s and Their Gas Transport Properties. *J. Membr. Sci.* **2016**, *497*, 172–182. [[CrossRef](#)]
70. Zang, Y.; Aoki, T.; Teraguchi, M.; Kaneko, T.; Jia, H.; Ma, L.; Miao, F. New Synthetic Methods of Novel Nanoporous Polycondensates and Excellent Oxygen Permselectivity of Their Composite Membranes. *Nanomaterials* **2019**, *9*, 859. [[CrossRef](#)]
71. Zhang, M.; Aoki, T.; Liu, L.; Wang, J.; Teraguchi, M.; Kaneko, T. Ultrahigh Oxygen Permeability of Chemically-Modified Membranes of Novel (Co)polyacetylenes Having a Photodegradative Backbone and Crosslinkable Side Chains. *Polymer* **2018**, *149*, 117–123. [[CrossRef](#)]
72. Sakaguchi, T.; Shinoda, Y.; Hashimoto, T. Synthesis and Gas Permeability of Nitrated and Aminated Poly(diphenylacetylene)s. *Polymer* **2014**, *55*, 6680–6685. [[CrossRef](#)]
73. Sakaguchi, T.; Lin, Y.; Hashimoto, T. Enhancement of oxygen permeability by copolymerization of silyl group-containing diphenylacetylenes with tert-butyl group-containing diphenylacetylene and desilylation of copolymer membranes. *RSC Adv.* **2017**, *7*, 30949–30955. [[CrossRef](#)]
74. Xu, C.; Aoki, T.; Ma, L.; Jia, H.; Teraguchi, M.; Kaneko, T. Synthesis and Ultrahigh Oxygen Permeability of Silicon-containing cis-cisoidal Poly(substituted phenylacetylene)s. *Chem. Lett.* **2018**, *47*, 1314–1317. [[CrossRef](#)]

75. Qu, Y.; Du, X.; Cheng, K.; Zang, Y.; Xu, L.; Shinohara, K.-I.; Teraguchi, M.; Kaneko, T.; Aoki, T. Synthesis and Permselectivity of a Soluble Two-Dimensional Macromolecular Sheet by Solid–Solid Interfacial Polycondensation Followed by Chemical Exfoliation. *ACS Mater. Lett.* **2020**, *2*, 1121–1128. [[CrossRef](#)]
76. Wang, J.; Aoki, T.; Kaneko, T.; Teraguchi, M. Synthesis, In-Situ Membrane Preparation, and Good Gas Permselectivity of Insoluble Poly(substituted acetylene)s Loosely Cross-Linked with Short and Soft Siloxane and Silanol Linkages. *Polymer* **2019**, *187*, 122081. [[CrossRef](#)]
77. Wang, J.; Li, J.; Aoki, T.; Kaneko, T.; Teraguchi, M.; Shi, Z.; Jia, H. Subnanoporous Highly Oxygen Permselective Membranes from Poly(conjugated hyperbranched macromonomer)s Synthesized by One-Pot Simultaneous Two-Mode Homopolymerization of 1,3-Bis(silyl)phenylacetylene Using a Single Rh Catalytic System: Control of Their Structures and Permselectivities. *Macromolecules* **2017**, *50*, 7121–7136. [[CrossRef](#)]
78. Zang, Y.; Aoki, T.; Tanagi, H.; Matsui, K.; Teraguchi, M.; Kaneko, T.; Ma, L.; Jia, H.; Shinohara, K.-I. Synthesis of Two Well-Defined Quadruple-Stranded Copolymers having Two Kinds of Backbones by Postpolymerization of a Helical Template Polymer. *Macromol. Rapid Commun.* **2017**, *39*, 1700556. [[CrossRef](#)] [[PubMed](#)]
79. Sato, T.; Teraguchi, M.; Kiuchi, M.; Kaneko, T.; Aoki, T. Quantitative Introduction of Perfluoroalkyl Groups to Poly(diphenylacetylene) Membranes via Three-step Membrane Reaction Including Click Reaction and Their Gas Permeability. *Chem. Lett.* **2015**, *44*, 1679–1681. [[CrossRef](#)]
80. Xu, S.; Aoki, T.; Teraguchi, M.; Kaneko, T. High Oxygen Permselectivity through a Membrane from Novel Soluble Imido-bridged Ladder Polysiloxane. *Chem. Lett.* **2016**, *45*, 424–426. [[CrossRef](#)]
81. Kim, S.; Lee, Y.M. Rigid and Microporous Polymers for Gas Separation Membranes. *Prog. Polym. Sci.* **2015**, *43*, 1–32. [[CrossRef](#)]
82. Kiyono, M.; Williams, P.J.; Koros, W.J. Effect of Polymer Precursors on Carbon Molecular Sieve Structure and Separation Performance Properties. *Carbon* **2010**, *48*, 4432–4441. [[CrossRef](#)]
83. Hu, C.-P.; Polintan, C.K.; Tayo, L.L.; Chou, S.-C.; Tsai, H.-A.; Hung, W.-S.; Hu, C.-C.; Lee, K.-R.; Lai, J.-Y. The gas separation performance adjustment of carbon molecular sieve membrane depending on the chain rigidity and free volume characteristic of the polymeric precursor. *Carbon* **2018**, *143*, 343–351. [[CrossRef](#)]
84. Ma, X.; Swaidan, R.; Teng, B.; Tan, H.; Salinas, O.; Litwiller, E.; Han, Y.; Pinnau, I. Carbon Molecular Sieve Gas Separation Membranes Based on an Intrinsically Microporous Polyimide Precursor. *Carbon* **2013**, *62*, 88–96. [[CrossRef](#)]
85. Kita, H.; Yoshino, M.; Tanaka, K.; Okamoto, K.-I. Gas Permselectivity of Carbonized Polypyrrolone Membrane. *Chem. Commun.* **1997**, 1051–1052. [[CrossRef](#)]
86. Singh-Ghosal, A.; Koros, W.J. Air Separation Properties of Flat Sheet Homogeneous Pyrolytic Carbon Membranes. *J. Membr. Sci.* **2000**, *174*, 177–188. [[CrossRef](#)]
87. Rao, P.S.; Wey, M.-Y.; Tseng, H.-H.; Kumar, I.A.; Weng, T.-H. A Comparison of Carbon/Nanotube Molecular Sieve Membranes with Polymer Blend Carbon Molecular Sieve Membranes for the Gas Permeation Application. *Microporous Mesoporous Mater.* **2008**, *113*, 499–510. [[CrossRef](#)]
88. Kim, Y.K.; Lee, J.M.; Park, H.B.; Lee, Y.M. The Gas Separation Properties of Carbon Molecular Sieve Membranes Derived from Polyimides Having Carboxylic Acid Groups. *J. Membr. Sci.* **2004**, *235*, 139–146. [[CrossRef](#)]
89. Zhou, W.; Yoshino, M.; Kita, H.; Okamoto, K.-I. Preparation and Gas Permeation Properties of Carbon Molecular Sieve Membranes Based on Sulfonated Phenolic Resin. *J. Membr. Sci.* **2003**, *217*, 55–67. [[CrossRef](#)]
90. Kim, Y.K.; Park, H.B.; Lee, Y.M. Carbon molecular sieve membranes derived from thermally labile polymer containing blend polymers and their gas separation properties. *J. Membr. Sci.* **2004**, *243*, 9–17. [[CrossRef](#)]
91. Li, F.Y.; Xiao, Y.; Chung, T.-S.; Kawi, S. High-Performance Thermally Self-Cross-Linked Polymer of Intrinsic Microporosity (PIM-1) Membranes for Energy Development. *Macromolecules* **2012**, *45*, 1427–1437. [[CrossRef](#)]
92. Zhang, B.; Wang, T.; Wu, Y.; Liu, Q.; Liu, S.; Zhang, S.; Qiu, J. Preparation and Gas Permeation of Composite Carbon Membranes from Poly(phthalazinone ether sulfone ketone). *Sep. Purif. Technol.* **2008**, *60*, 259–263. [[CrossRef](#)]
93. Barsema, J.; Balster, J.; Jordan, V.; van der Vegt, N.; Wessling, M. Functionalized Carbon Molecular Sieve membranes containing Ag-nanoclusters. *J. Membr. Sci.* **2003**, *219*, 47–57. [[CrossRef](#)]
94. Wey, M.-Y.; Tseng, H.-H.; Chiang, C.-K. Effect of MFI zeolite intermediate layers on gas separation performance of carbon molecular sieve (CMS) membranes. *J. Membr. Sci.* **2013**, *446*, 220–229. [[CrossRef](#)]
95. Hosseini, S.S.; Omidkhah, M.R.; Moghaddam, A.Z.; Pirouzfard, V.; Krantz, W.; Tan, N.R. Enhancing the Properties and Gas Separation Performance of PBI–Polyimides Blend Carbon Molecular Sieve Membranes via Optimization of the Pyrolysis Process. *Sep. Purif. Technol.* **2014**, *122*, 278–289. [[CrossRef](#)]
96. Kim, Y.K.; Park, H.B.; Lee, Y.M. Preparation and characterization of carbon molecular sieve membranes derived from BTDA–ODA polyimide and their gas separation properties. *J. Membr. Sci.* **2005**, *255*, 265–273. [[CrossRef](#)]
97. Yoshimune, M.; Fujiwara, I.; Haraya, K. Carbon Molecular Sieve Membranes Derived from Trimethylsilyl Substituted Poly(phenylene oxide) for Gas Separation. *Carbon* **2007**, *45*, 553–560. [[CrossRef](#)]
98. Park, H.B.; Lee, Y.M. Pyrolytic Carbon–Silica Membrane: A Promising Membrane Material for Improved Gas Separation. *J. Membr. Sci.* **2003**, *213*, 263–272. [[CrossRef](#)]
99. Suda, H.; Haraya, K. Gas Permeation through Micropores of Carbon Molecular Sieve Membranes Derived from Kapton Polyimide. *J. Phys. Chem. B* **1997**, *101*, 3988–3994. [[CrossRef](#)]

100. Steel, K.M.; Koros, W.J. Investigation of Porosity of Carbon Materials and Related Effects on Gas Separation Properties. *Carbon* **2003**, *41*, 253–266. [[CrossRef](#)]
101. Zhang, C.; Koros, W.J. Ultrasensitive Carbon Molecular Sieve Membranes with Tailored Synergistic Sorption Selective Properties. *Adv. Mater.* **2017**, *29*, 1701631. [[CrossRef](#)] [[PubMed](#)]
102. Zhang, B.; Wang, T.; Liu, S.; Zhang, S.; Qiu, J.; Chen, Z.-G.; Cheng, H. Structure and Morphology of Microporous Carbon Membrane Materials Derived from Poly(Phthalazinone Ether Sulfone Ketone). *Microporous Mesoporous Mater.* **2006**, *96*, 79–83. [[CrossRef](#)]
103. Wang, T.; Zhang, B.; Qiu, J.; Wu, Y.; Zhang, S.; Cao, Y. Effects of Sulfone/Ketone in Poly(phthalazinone ether sulfone ketone) on the Gas Permeation of Their Derived Carbon Membranes. *J. Membr. Sci.* **2009**, *330*, 319–325. [[CrossRef](#)]
104. Chung, T.-S.; Jiang, L.Y.; Li, Y.; Kulprathipanja, S. Mixed matrix membranes (MMMs) Comprising Organic Polymers with Dispersed Inorganic Fillers for Gas Separation. *Prog. Polym. Sci.* **2007**, *32*, 483–507. [[CrossRef](#)]
105. Dechnik, J.; Gascon, J.; Doonan, C.J.; Janiak, C.; Sumbly, C.J. Mixed-Matrix Membranes. *Angew. Chem. Int. Ed.* **2017**, *56*, 9292–9310. [[CrossRef](#)] [[PubMed](#)]
106. Park, H.B.; Kamcev, J.; Robeson, L.M.; Elimelech, M.; Freeman, B.D. Maximizing the Right Stuff: The Trade-Off between Membrane Permeability and Selectivity. *Science* **2017**, *356*, eaab0530. [[CrossRef](#)]
107. Slater, A.G.; Cooper, A.I. Function-led Design of New Porous Materials. *Science* **2015**, *348*, 8075. [[CrossRef](#)] [[PubMed](#)]
108. Wang, H.; Holmberg, B.A.; Yan, Y. Homogeneous Polymer-zeolite Nanocomposite Membranes by Incorporating Dispersible Template-removed Zeolitenanocrystals. *J. Mater. Chem.* **2002**, *12*, 3640–3643. [[CrossRef](#)]
109. Li, Y.; Chung, T.-S.; Cao, C.; Kulprathipanja, S. The Effects of Polymer Chain Rigidity, Zeolite Pore Size and Pore Blockage on Polyethersulfone (PES)-Zeolite A Mixed Matrix Membranes. *J. Membr. Sci.* **2005**, *260*, 45–55. [[CrossRef](#)]
110. Xin, Q.; Liu, T.; Li, Z.; Wang, S.; Li, Y.; Li, Z.; Ouyang, J.; Jiang, Z.; Wu, H. Mixed Matrix Membranes Composed of Sulfonated Poly(ether ether ketone) and a Sulfonated Metal-Organic Framework for Gas Separation. *J. Membr. Sci.* **2015**, *488*, 67–78. [[CrossRef](#)]
111. Anjum, M.W.; Bueken, B.; De Vos, D.; Vankelecom, I.F. MIL-125(Ti) Based Mixed Matrix Membranes for CO₂ Separation from CH₄ and N₂. *J. Membr. Sci.* **2016**, *502*, 21–28. [[CrossRef](#)]
112. Anjum, M.W.; Vermoortele, F.; Khan, A.L.; Bueken, B.; De Vos, D.E.; Vankelecom, I.F.J. Modulated UiO-66-Based Mixed-Matrix Membranes for CO₂ Separation. *ACS Appl. Mater. Interfaces* **2015**, *7*, 25193–25201. [[CrossRef](#)] [[PubMed](#)]
113. Wang, H.; He, S.; Qin, X.; Li, C.; Li, T. Interfacial Engineering in Metal–Organic Framework-Based Mixed Matrix Membranes Using Covalently Grafted Polyimide Brushes. *J. Am. Chem. Soc.* **2018**, *140*, 17203–17210. [[CrossRef](#)] [[PubMed](#)]
114. Bushell, A.F.; Budd, P.M.; Attfield, M.P.; Jones, J.T.A.; Hasell, T.; Cooper, A.I.; Bernardo, P.; Bazzarelli, F.; Clarizia, G.; Jansen, J.C. Nanoporous Organic Polymer/Cage Composite Membranes. *Angew. Chem. Int. Ed.* **2012**, *52*, 1253–1256. [[CrossRef](#)]
115. Jiang, L.Y.; Chung, T.S. β -Cyclodextrin Containing Matrimid[®] Sub-Nanocomposite Membranes for Pervaporation Application. *J. Membr. Sci.* **2009**, *327*, 216–225. [[CrossRef](#)]
116. Bachman, J.E.; Smith, Z.P.; Li, T.; Xu, T.; Long, J.R. Enhanced Ethylene Separation and Plasticization Resistance in Polymer Membranes Incorporating Metal-Organic Framework Nanocrystals. *Nat. Mater.* **2016**, *15*, 845–850. [[CrossRef](#)]
117. Peng, Y.; Li, Y.; Ban, Y.; Jin, H.; Jiao, W.; Liu, X.; Yang, W. Metal-Organic Framework Nanosheets as Building Blocks for Molecular Sieving Membranes. *Science* **2014**, *346*, 1356–1359. [[CrossRef](#)]
118. Kang, Z.; Peng, Y.; Hu, Z.; Qian, Y.; Chi, C.; Yeo, L.Y.; Tee, L.; Zhao, D. Mixed Matrix Membranes Composed of Two-Dimensional Metal–Organic Framework Nanosheets for Pre-Combustion CO₂ Capture: A Relationship Study of Filler Morphology versus Membrane Performance. *J. Mater. Chem. A* **2015**, *3*, 20801–20810. [[CrossRef](#)]
119. Rodenas, T.; Luz, I.; Prieto, G.; Seoane, B.; Miro, H.; Corma, A.; Kapteijn, F.; Xamena, F.X.L.I.; Gascon, J. Metal-Organic Framework Nanosheets in Polymer Composite Materials for Gas Separation. *Nat. Mater.* **2015**, *14*, 48–55. [[CrossRef](#)]
120. Nishide, H.; Ohyanagi, M.; Okada, O.; Tsuchida, E. Dual-Mode Transport of Molecular Oxygen in a Membrane Containing a Cobalt Porphyrin Complex as a Fixed Carrier. *Macromolecules* **1987**, *20*, 417–422. [[CrossRef](#)]
121. Song, Q.; Cao, S.; Pritchard, R.H.; Ghalei, B.; Al-Muhtaseb, S.A.; Terentjev, E.; Cheetham, A.K.; Sivaniah, E. Controlled Thermal Oxidative Crosslinking of Polymers of Intrinsic Microporosity towards Tunable Molecular Sieve Membranes. *Nat. Commun.* **2014**, *5*, 4813. [[CrossRef](#)] [[PubMed](#)]
122. Song, Q.; Cao, S.; Zavala-Rivera, P.; Lu, L.P.; Li, W.; Ji, Y.; Al-Muhtaseb, S.A.; Cheetham, A.K.; Sivaniah, E. Photo-oxidative Enhancement of Polymeric Molecular Sieve Membranes. *Nat. Commun.* **2013**, *4*, 1918. [[CrossRef](#)] [[PubMed](#)]
123. Kim, H.W.; Yoon, H.W.; Yoon, S.-M.; Yoo, B.M.; Ahn, B.K.; Cho, Y.H.; Shin, H.J.; Yang, H.; Paik, U.; Kwon, S.; et al. Selective Gas Transport Through Few-Layered Graphene and Graphene Oxide Membranes. *Science* **2013**, *342*, 91–95. [[CrossRef](#)]
124. Li, H.; Song, Z.; Zhang, X.; Huang, Y.; Li, S.; Mao, Y.; Ploehn, H.J.; Bao, Y.; Yu, M. Ultrathin, Molecular-Sieving Graphene Oxide Membranes for Selective Hydrogen Separation. *Science* **2013**, *342*, 95–98. [[CrossRef](#)]
125. Ding, S.-Y.; Wang, W. Covalent organic frameworks (COFs): From design to applications. *Chem. Soc. Rev.* **2013**, *42*, 548–568. [[CrossRef](#)] [[PubMed](#)]
126. Zheng, Z.; Grüner, R.; Feng, X. Synthetic Two-Dimensional Materials: A New Paradigm of Membranes for Ultimate Separation. *Adv. Mater.* **2016**, *28*, 6529–6545. [[CrossRef](#)]